



UNIVERSITY OF ICELAND

GRO • GTP
Geothermal
Training
Programme



M.S. Thesis
in Earth Science

Scaling Potential During Utilization of High Temperature Saline Fluids in the Assal Geothermal Area (Djibouti)

Idil Souleiman Bouraleh

February 2024

Scaling Potential During Utilization of High Temperature Saline Fluids in the Assal Geothermal Area (Djibouti)

Idil Souleiman Bouraleh

Dissertation submitted in partial fulfillment of a
Magister Scientiarum degree in Geology

M.S. Committee
Halldór Ármannsson
Iwona Monika Galeczka
Daniel Villarroel-Camacho

Examiner
Þráinn Friðriksson

Faculty of Earth Sciences
School of Engineering and Natural Sciences
University of Iceland
Reykjavik, February 2024

Scaling Potential During Utilization of High Temperature Saline Fluids in the Assal
Geothermal Area (Djibouti)

Scale Potential of high temperature saline fluids in Assal, Djibouti

60 ECTS Dissertation submitted in partial fulfilment of an *M.S.* degree in Geology

Copyright © 2024 Idil Souleiman Bouraleh
All rights reserved.

Faculty of Earth Sciences
School of Engineering and Natural Sciences
University of Iceland
Sturlugata 7
101, Reykjavik
Iceland

Telephone: 525 4000

Bibliographic information:

Idil Souleiman, 2024, *Scaling Potential During Utilization of High Temperature Saline Fluids in the Assal Geothermal Area (Djibouti)*, M.S. thesis, Faculty of Earth Science, University of Iceland, 59 pp.

Abstract

The geochemical compositions and scaling potential fluids from the Assal geothermal system in Djibouti were studied through the analysis of five samples, including the fluids discharged from the Assal wells, Lake Assal and Ghoubbet seawater. The chemical composition and mineral saturation index assuming both boiled and cooled scenarios were calculated using the speciation software WATCH and PHREEQC. The deep reservoir temperature ranged between 245°C - 251°C, assuming equilibrium with quartz. The chloride concentration, approximately 70,000 mg/kg, is three to four times higher than that of the Ghoubbet seawater (20,800 mg/kg). During adiabatic cooling, galena, amorphous silica and sphalerite were calculated to precipitate in accordance with composition of the scale samples. In contrast, ferrosilite and calcite were predicted to form in the boiling model.

Fe is more prevalent in the observed and predicted mineral precipitation than Mn, Pb, and Zn, except for sulfide minerals, which may be impacted by surface mineral deposition. The conductive cooling model simulates the mineral precipitation observed in the scale deposit better. This study shows that scales formed during geothermal utilization in Assal (galena, amorphous silica, ferrosilite) are similar to those found in other geothermal areas such as Reykjanes, Salton Sea, and Milos. These high salinity geothermal fluids could be utilized not only for electricity and heat production but also for critical and valuable metal and nonmetal extraction. The potential mass of recovered Li is calculated to be 68,900 t/month, SiO₂ 215,000 t/month, Mn 86,000 t/month, Pb 581 t/month, Zn 17,300 t/month and Fe 43,000 t/month.

Útdráttur

Jarðefnafræðileg samsetning og möguleikar á útfellingum í jarðhitavökva á Assal svæðinu í Djibouti voru rannsökuð með greiningu á fimm sýnum, þar á meðal úr borholum á Assal svæðinu, Lake Assal stöðuvatninu og Ghoubbet-flóanum. Efnasamsetning og mettunarstuðull steinefna sem gera ráð fyrir bæði suðu og kælingu, voru reiknuð út með WATCH og PHREEQC hugbúnaðinum. Hitastig jarðhitakerfisins var á bilinu 245°C - 251°C miðað við að gert væri ráð fyrir jafnvægi við kvars. Klórídstyrkurinn, um 70.000 mg/kg, er þrisvar til fjórum sinnum meiri en í Ghoubbet-flóanum (20.800 mg/kg). Við innræna kælingu var reiknað út að galena, myndlaus kísill og sphalerít féllu út í samræmi við samsetningu sýnanna. Aftur á móti var gert ráð fyrir að járnslít og kalsít mynduðust í suðulíkaninu. Fe var algengara í steinefnaútfellingu en Mn, Pb og Zn, fyrir utan brennisteinssteindir, sem geta orðið fyrir áhrifum af jarðefnaútfellingu á yfirborðinu. Leiðandi kælilíkanið líkti betur eftir útfellingu steinefna sem sáust í útfellingunum. Þessi rannsókn sýnir að þær útfellingar sem myndast við jarðhitanytingu á Assal svæðinu (galena, myndlaus kísill, ferrósilít) eru svipaðar þeim sem má finna á öðrum jarðhitasvæðum eins og Reykjanesi, Salton Sea og Milos. Þennan salta jarðhitavökva væri ekki aðeins hægt að nýta til raforku- og hitaframleiðslu heldur einnig til að vinna mikilvæga og verðmæta málma og málmleysingja. Mögulegt væri að vinna 68.900 t/mán af Li, 215.000 t/mán af SiO₂, 86.000 t/mán af Mn, 581 t/mán af Pb, 17.300 t/mán af Zn og 43.000 t/mán af Fe.

Dedicated

to my beloved parents, Souleiman and Safia, for their encouragement and inspiration

Table of Contents

List of Figures	x
List of Tables.....	xi
Appendix	xii
Acknowledgements	xiii
1 Introduction.....	15
2 Assal geothermal area	17
2.1 Geological setting.....	17
2.2 Geothermal exploration.....	18
2.3 Characteristics of the fluid	20
2.4 Well logging and lithology.....	20
2.5 Scale formation.....	21
3 Methods.....	25
3.1 Equipment	25
3.2 Sampling and analysis	27
3.3 Data analysis.....	27
3.3.1 Reservoir fluid composition.....	27
3.3.2 Mineral saturation	28
4 Results and Discussion.....	29
4.1 Surface fluid compositions.....	29
4.2 Deep fluid composition	31
4.3 Mineral saturation.....	32
4.3.1 Silica mineral saturation	32
4.3.2 Sulfate mineral saturation	34
4.3.3 Sulfide mineral saturation.....	35
4.3.4 Carbonate Mineral saturation.....	37
4.3.5 Oxide Minerals saturation.....	38
4.3.6 Other mineral saturation	40
4.4 Trace elements.....	42
4.5 Comparison between similar fields	44
4.6 Mineral extraction	47
5 Conclusions	49
References.....	50

List of Figures

Figure 1: Geological map of the Assal geothermal field including the MT data (from Hassan et al., 2021).	17
Figure 2: Regional map of Assal wells, Fiale wells, Fiale caldera as well as regional faults (Le Gall, et al. (2015) in Carver et al. (2019)).....	18
Figure 3: The lithology, the temperature and pressure profiles of well Assal 3	21
Figure 4: Sulfide (galena (PbS)) and iron silicate (FeSiO ₃) on a deposition coupon (Ármannsson et al., 1990)	22
Figure 5: Scale deposition rate on coupons at different pressures of Assal 3. (modified from Virkir-Orkint, 1990)	24
Figure 6: a) Dosage pumps for sulfide inhibitors; b) Iron silicates and calcium chloride pseudo scales on a deposition coupon (Ármannsson et al., 1990).	24
Figure 7: Equipment setup for testing scaling and corrosion on the Assal 3 modified by Virkir-Orkint, 1990.	25
Figure 8: Saturation state with respect to silica minerals upon boiling (solid line) and cooling (dotted line).	33
Figure 9: pH and Fe (OH) ⁻⁴ activity ratios plots versus aquifer temperature.....	34
Figure 10: Saturation state with respect to sulfate minerals upon boiling (solid line) and cooling (dotted line).....	35
Figure 11: Saturation state with respect to sulfide minerals upon boiling (solid line) and cooling (dotted line).....	36
Figure 12: Saturation state with respect to carbonate minerals upon boiling (solid line) and cooling (dotted line).....	38
Figure 13: Saturation state with respect to oxide minerals upon boiling (solid line) and cooling (dotted line).	39
Figure 14: Saturation state with respect to epitote, low albite, witherite and illite minerals upon boiling (solid line) and cooling (dotted line).	40
Figure 15: Saturation indices (SI) with respect to silica, sulfide, sulfate, carbonate, oxide and other calculated from Assal aquifer fluid upon adiabatic boiling (red colour) and cooling model (green colours).....	42
Figure 16: Mineral saturation of Assal 3 aquifer fluids with respect to Fe, Pb, Mn and Zn trace elements minerals. Different types of minerals are presented such as sulfide (in orange and green), oxide (in black), carbonate (blue circle) and silica (in yellow).	43

List of Tables

Table 1: Characteristics of geothermal wells in the Assal and Fiale area (Cheik, 2010; Turk et al., 2019).	19
Table 2: The conditions at which scales formed in Assal 3 (Virkir-Orkint, 1990).....	23
Table 3: Analytical methods applied for studying of the fluids from Assal 3 well (Virkir-Orkint, 1990).....	26
Table 4: The chemical compositions of the fluids discharged from well Assal 3, Ghoubbet seawater and Lake Assal (Virkir-Orkint, 1990).....	29
Table 5: Deep aquifer fluid compositions of Assal geothermal wells. (Concentrations are given in mg/kg).....	31
Table 6: Comparison between model and field observations regarding the scales.	41
Table 7: Comparison of downhole liquid composition in Reykjanes, Salton Sea, Milos, and Assal.....	44
Table 8: Comparison between the mineral depositions found in Reykjanes (Iceland); Salton Sea (California); Milos (Greece) and Assal (Djibouti).	46
Table 9: Estimation of mineral/extraction from the Assal fluids.	48

List of Appendix

Appendix A: Chemical composition of the scaling encountered in the well Assal 3 (Haga, 2015).....	57
Appendix B: Temperature equations for equilibrium constants for individual mineral dissolution reactions. The log K is valid in the range 0-300°C (Parkhurst and Appelo, 1999).	58

Acknowledgements

My sincere gratitude goes to the Government of Iceland through the GRÓ Geothermal Training Programme (GRÓ-GTP) under the auspices of the United Nations Educational, Scientific and Cultural Organization (UNESCO) for the financial support that enabled me to succeed in this project and advance in my professional career.

For allowing me to begin and complete the master's program at the University of Iceland, I would like to extend my sincere gratitude to Guðni Axelsson, the current director of GRÓ-GTP, and to Ludvik Georgsson, the former director of United Nations University (UNU-GTP). Ingimar Haraldsson, Vigdís Harðardóttir, Markús Wilde, and to the special one Málfríður Ómarsdóttir I would like to thank all of you for all your assistance and encouragement in many circumstances. I want to thank Dr. Kayad Moussa, General Manager of Office Djiboutien de Développement de l'Énergie Géothermique (ODDEG), for allowing me to continue my master's study and for the support and encouragement not only during my studies in Iceland but also in my professional career.

My appreciation goes to my supervisors Halldór Ármannsson, Iwona Monika Galeczka and Daniel Villarroel-Camacho for their thoughtful guidance, experience and time invested in the knowledge-sharing process during my study.

I would like to thank my friends from GRÓ-GTP for the wonderful times, laughs, memories, support, and friendship during my stay in Iceland. More specially, Frida and Daniel, I want to thank you for every help, advice, and encouragement as well as for being a solid friend who constantly keeps me motivated to pursue my goals. Thanks to my friends from my home country, Djibouti, for their support.

Finally, I would like to give my profound thanks to my beloved family for all of their encouragement, love, support, and prayers during my studies. All gratitude goes to God for continuing to bless me each day.

1 Introduction

Geothermal energy represents a renewable energy source capable of generating and/or provide both electrical power and heat. In recent decades, there has been a growing interest in geothermal energy as a viable alternative to fossil fuels. This is due to a number of factors, including the increasing cost of fossil fuels, the environmental concerns associated with fossil fuel use, and the technological advances that have made geothermal energy more efficient and cost-effective (Alderson, 2023). Nonetheless, the application and harnessing of geothermal energy encounter several challenges, one of which is the occurrence of scaling (Ellis and Mahon, 1977; Corsi, 1986; Gunnlaugsson, 2012; Gunnlaugsson et al., 2014; Zhao et al., 2022).

Scaling is the deposition of minerals from geothermal brines on surfaces, including but not limited to heat exchangers and pipelines. Such mineral deposition can significantly reduce the performance of geothermal power plants and result in equipment failures, efficiency loss, equipment damage, higher maintenance costs, and environmental implications (Gunnarsson and Arnórsson, 2005). The scaling potential of geothermal separated water (SGW) depends on a few factors, including its chemistry, temperature and pressure, and the construction materials used in the geothermal surface and subsurface installations. The most common types of scales observed in geothermal wells and installations are carbonate minerals (calcite and aragonite), amorphous silica, metal oxides and sulfides (Arnórsson, 1981; 1989; Brown and Dunstall, 2000; Sigfússon and Gunnarsson, 2011).

The reduction or prevention of mineral depositions is frequently accomplished using anti-scalants (Zotzman et al., 2023). However, these scaling inhibitors have some disadvantages including high costs, variable inhibitory performance in geothermal fluids with diverse chemical and physical characteristics, and uncertainties regarding their long-term effects within the reservoir. An alternative approach for scale prevention could be the continuous partial removal of the scale-forming metal ions from the fluid so that the concentration of these ions is lowered below the respective mineral saturation at the given conditions (Graham et al., 2003; Zotzmann et al., 2018).

The extraction of these minerals and metals from geothermal fluids can be viewed as "solution mining by nature" considering the use of new hydro-metallurgical techniques for isolation and purification, among others (Bourcier et al., 2005). The quantity of recoverable minerals in brines can be substantial, even considering their relatively low concentrations. For example, it is estimated that approximately 30 kg of metals passes daily through the facilities of a 50 MWe power plant (Gallup, 1998), considering the composition of typical geothermal waters.

Furthermore, mineral recovery is the extraction of different minerals from geothermal brines offering two benefits: (i) mitigation of environmental impacts associated with brine discharge and (ii) the commercialization of the extracted minerals (Toba et al., 2021). The most common minerals in brines include SiO₂, B, Sr, Zn, K, Mg, Mn, Ba, Li, and rare earth elements, among others. The first attempt to recover B from geothermal fluids dates to 1818

in Larderello, Italy. Following to this pioneering effort, various techniques have been developed in different locations around the world, these techniques include:

- SiO₂ extraction: In the mid-1990s, a proposal emerged for a Silica production pilot plant in Wairakei, New Zealand. Despite successful tests conducted on a large pilot plant, the project did not progress further for commercial purposes (Mroczek et al., 2015).
- Zn extraction: CalEnergy proposed the construction of a mineral recovery facility to process geothermal fluid from multiple power plants in the US. The aim was producing 30,000 tons of Zn at 99% purity. Initial production started in 2002 and continued until 2004 when the project was terminated due to economic reasons (Warren, 2021).
- Li extraction: EnergySource (Warren, 2021) reported the successful completion of pilot testing for their patented Integrated Lithium Adsorption Desorption (ILiAD) technology, demonstrating a lithium recovery rate more than 90%. Consequently, preparations are in progress to launch a new Li-extraction facility, scheduled to start operations in 2023.

The objective of this project is to study the scaling potential associated to the high-temperature geothermal fluids present in the Assal geothermal field. A total of six exploration wells were within the study area. However, it is noteworthy that only two of these wells, Assal 3 and Assal 6, were considered as productive wells. Subsequently, Assal 6 was exclusively utilized for the monitoring of the reservoir water level during the scaling and corrosion studies performed in well Assal 3. These studies demonstrated the deposition of sulfides and iron silicates in the well, and the formation of silica scales in the surface equipment (Virikir-Orkint, 1990). Other studies, e.g., (Ármansson and Hardardóttir, 2010) have shown that sulfide formation may be chemically inhibited, whereas the iron silicate deposition can be prevented by keeping the wellhead pressure well above 16 bar. The amorphous silica deposition can be limited by keeping the separator pressure above the saturation pressure of amorphous silica.

This study consists of characterization of the discharged fluids in Assal by reconstructing the chemical composition of the reservoir fluid and calculating the saturation state of minerals formed during the utilization upon boiling and cooling. Furthermore, an evaluation in Fe-Mg-Pb-Zn-bearing minerals was conducted to evaluate their scaling potential and metal extraction considering the thermo-economics characteristics of the fluids and the region.

2 Assal geothermal area

2.1 Geological setting

The Assal Rift area is the most active tectonic field in the Republic of Djibouti, and it is situated approximately 120 kilometres from the capital city. Positioned at the convergence point of the African Rift, the Gulf of Aden, and the Red Sea, the Assal Rift is marked by a continuous spreading motion of approximately 2 centimetres per year, providing clear surface evidence of the interactions between the Arabian and African tectonic plates (Tazieff et al., 1972; Barberi et al., 1970; Varet, 1978, 2014).

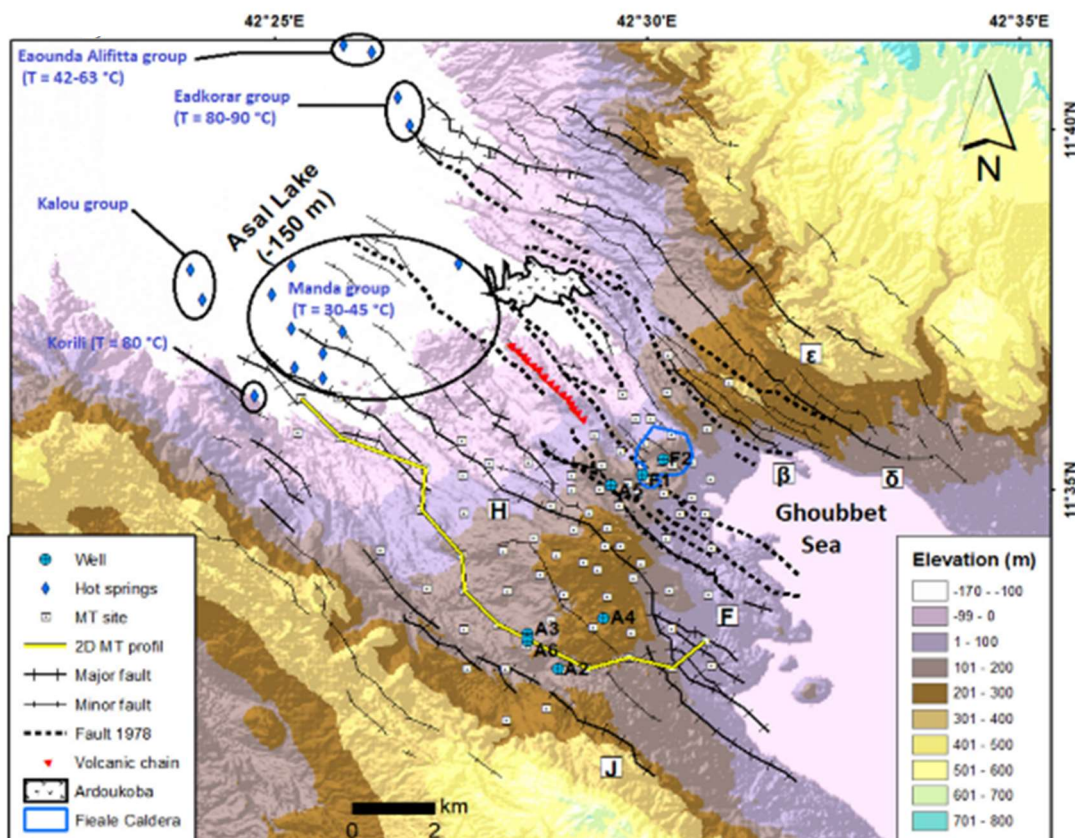


Figure 1: Geological map of the Assal geothermal field including the MT data (from Hassan et al., 2021).

According to Sanjuan (2010), the Assal Rift is about 9-10 km wide and spread from Lake Assal (150 m below sea level) to the NW from the Gulf of Ghoubbet-Al-Kharab to the SE. The most active part of the Assal Rift called by the Inner Rift hosted the latest volcano eruption in 1978. The fissure eruption (about 25 fissures) trend is parallel to the NW-SE of the Rift. The lava flowed to an area of more than 3 km² and has a thickness of 25 m. The inner rift is characterised by intense fracturing, recent lava flows and lake sediments (Global

volcanism program, 1978). There are several thermal springs and fumaroles among the area's surface manifestations (Figure 1).

2.2 Geothermal exploration

The first geothermal exploration in the Assal area was conducted by the Bureau de Recherches Géologiques et Minières (BRGM) and the Centre National de Recherche Scientifique (CNRS) in 1970. The results of these comprehensive geological, geochemical, and geophysical surveys demonstrated a large geothermal potential of the area, laying the groundwork for subsequent phases for the development of the area (drilling).

Following the surface exploration phase, the collaborative efforts of the Government of Djibouti and the United Nations Development Program (UNDP) culminated in the drilling of six geothermal wells, Assal 1 to Assal 6. These wells were drilled to depths ranging from 1147 to 2105 meters, as detailed in Table 1 (Hjartarson et al., 2010; Battisteili et al., 1990).

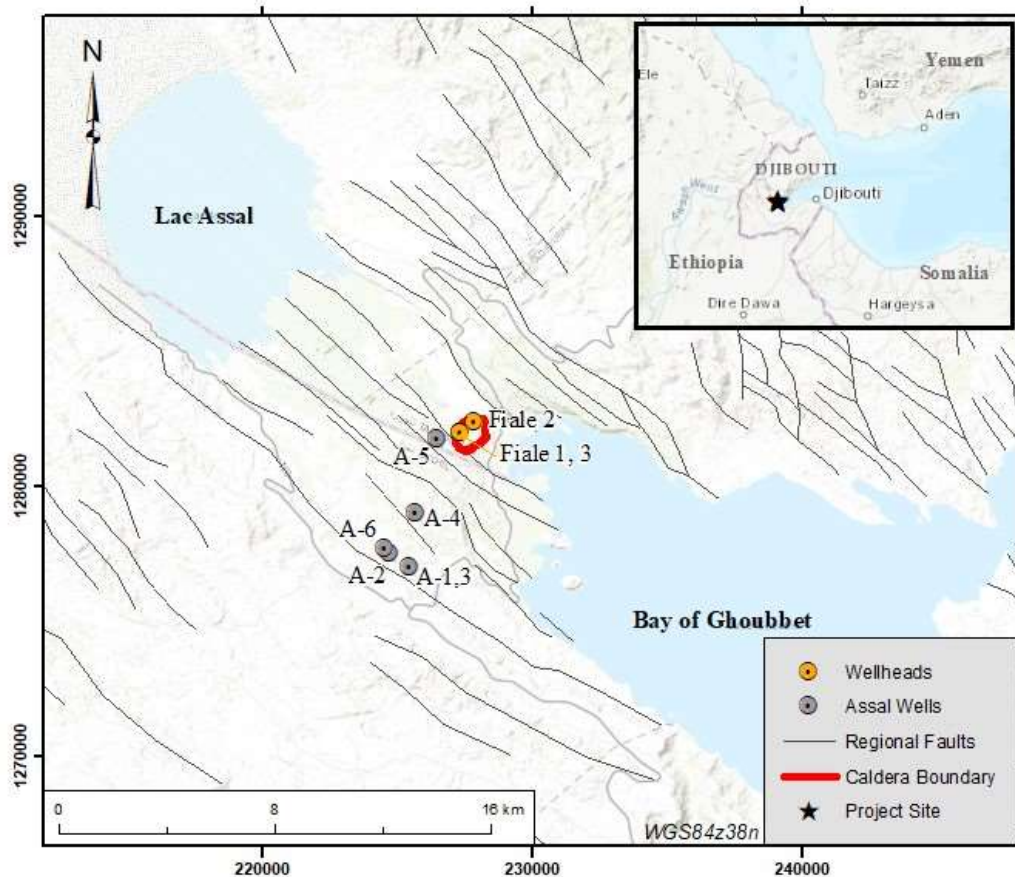


Figure 2: Regional map of Assal wells, Fiale wells, Fiale caldera as well as regional faults (Le Gall, et al. (2015) in Carver et al. (2019)).

Well Assal 1, with a depth of 1554 m, showed a feed zone temperature of approximately 260°C and produced 38 kg/s of two-phase fluid (Haga, 2015). On the other hand, well Assal 2 (1147 m depth) showed a subsurface temperature of approximately 235°C, although it did not yield productive results. In contrast, well Assal 6 (1716 m depth) was drilled 300 m

northwest of Assal 3 (1316 m depth) and was proved to be a productive well. The analysis of the fluid chemistry revealed similarities with Assal 1, suggesting that they share the same reservoir with temperature about 260 - 280°C. Wells Assal 4 (2013 m depth) and 5 (2105 m depth) had measured temperatures of 345°C and 359°C, respectively (Table 1). However, these wells were unproductive (Aqater, 1989).

In 2008, Reykjavik Energy Invest (REI) and the Government of Djibouti signed an agreement to develop a conceptual model of the area that could be used to site future exploration wells. (Houssein and Axelsson, 2010). This study identified three geothermal fields within the Assal area, specifically the Gale le Koma, Assal-Fiale, and South of Assal Lake. Subsequently, in 2018-2019, three-deep exploration wells (Fiale 1, 2 and 3) were drilled to depths of 2445-2743 m as a part of the geothermal exploration project in the Fiale Caldera (Figure 2). The main purpose was to build a geothermal power plant of 50 MWe capacity (Turk et al., 2019).

The Government of Djibouti, using Kuwaiti funding, decided to drill ten wells, encompassing eight production wells and two reinjection wells, with the aim of establishing a geothermal power plant with 15 MWe capacity. Kenya Electricity Generating Company (KenGen) has secured the contract to drill three geothermal wells in Assal region with the collaboration with the Djiboutian Office for Geothermal Energy Development (ODDEG) (Richter, A., 2021a)

Three of these wells will be drilled in Gale le Koma by the Kenya Electricity Generating Company (KenGen) after signing the contract with the Djiboutian Office for Geothermal Energy Development (ODDEG) (Richter, A., 2021a). **Error! Reference source not found.** shows the Assal wells, Fiale wells, Fiale caldera as well as regional faults locations in the Assal region.

Table 1: Characteristics of geothermal wells in the Assal and Fiale area (Cheik, 2010; Turk et al., 2019).

Wells	Date	Total Depth (m)	Temp (°C)
Assal 1	1975	1146	260
Assal 2	1975	1554	235
Assal 3	1987	1316	260
Assal 4	1987	2013	345
Assal 5	1988	2105	359
Assal 6	1988	1761	280
GLC*	2016	600	130
Fiale 1	2018	2743	363
Fiale 2	2019	2445	352
Fiale 3	2019	2625	362

*From internal report.

2.3 Characteristics of the geothermal fluid

The Assal geothermal region is characterized by number of thermal springs and fumaroles. The geothermal wells Assal 3 and Assal 6 have produced highly saline fluids characterized by a total dissolved solids content ranging from 115 g/l to 120 g/l, this concentration is approximately 3.5 times higher than sea water and the pH measurements fell within the range of 4 to 5.

Previous studies were undertaken by Lopoukhine (1973), Bosch et al. (1974), Fouillac et al. (1983), Fontes et al. (1989), Sanjuan (1990), and Varet (2014), and attempted to explain the origins of the thermal springs and geothermal reservoir fluids within the Assal region. Their studies were primarily directed at comprehending the sources and characteristics of the Assal geothermal system.

These studies have provided strong evidence that the geothermal fluids present in the Assal region are predominantly sourced by seawater, showing saturation with calcium sulfate (CaSO_4) and sodium chloride (NaCl). These fluids likely originated primarily from the Ghoubbet Pass, where they flow in a north-west to south-east direction, entering the South-east Lake Assal through fissures and open faults situated on the northern side of the rift. Finally, the chemical composition of the Assal geothermal fluids was interpreted as a combination of seawater-basaltic rock interaction and evaporation (Sanjuan, 1990).

2.4 Well logging and lithology

Between January and March 1990, temperature logs were conducted in flowing conditions. The measured flow from well Assal 3 was 31.2 kg/s at 19.2 bar well head pressure (WHP). The other wells (Assal 1, Assal 2, Assal 4 and Assal 5) were logged in static conditions (no flow).

The temperature logs show a cooling zone at depth of 400 to 600 m, characterized by an average temperature ranging from 135 to 180 °C (Figure 3). During drilling operations, notably permeable zones were identified at depths of 400 to 460 m and 540 to 553 m (Virkir-Orkint, 1990). Subsequently, a temperature above to 260°C was recorded from 600 m to 1180 m depth, indicating a low permeability.

Aquater (1989) identified three feed zones at depths of 1016-1316, 1225-1250 and approximately 1075 m. The fluid temperature zone is in the order of 265 °C. It is worth noting that as reported by Virkir-Orkint (1990), 70% of the discharged fluid originates from the feed zone below 1200 m. The static pressure profiles imply a drawdown of 6.5 to 6.9 bar in the reservoir. The flow rates range from 30.8 to 32.8 kg/s (111 to 118 tonnes per hour).

The main stratigraphic profile consists of three primary units: the Assal series, which involves basalts and hyaloclastites that are less than 1 Ma old; the Afar stratoid series, characterized by basalts with some rhyolites dated to be 4 Ma old; and the Dalha unit,

consisting of basaltic lava flows with some intercalations of rhyolites and trachyte dated as 4-9 Ma old (Aqwater, 1989).

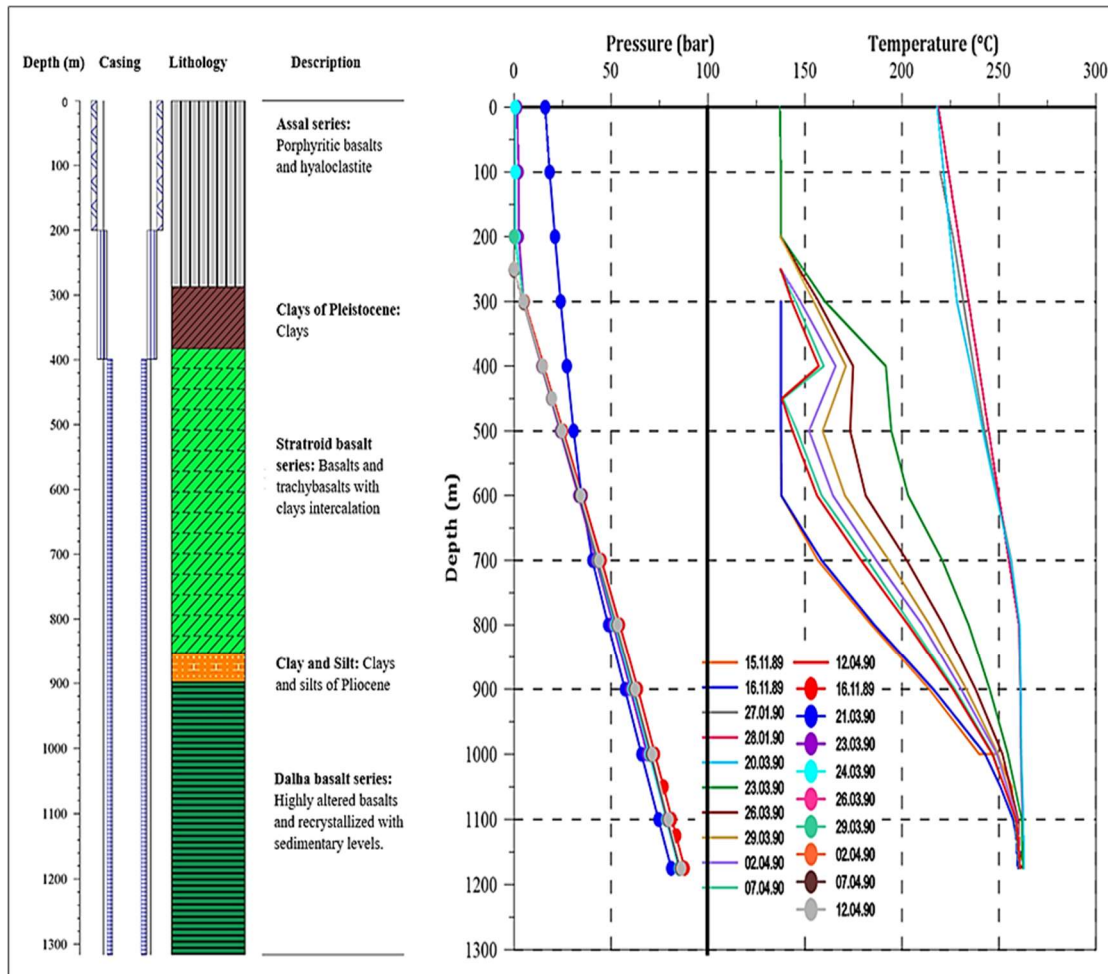


Figure 3: The lithology, temperature and pressure profiles of well Assal 3

2.5 Scale formation

As mentioned before, the scaling and corrosion studies of Assal 3 were carried out by Virkir-Orkint Consulting Group Ltd. Of Iceland in 1990. The Assal 3 well discharged 254,000 tons of fluid in total, with an average flow rate of 31.6 kg/s. Calliper logs indicate that a deposited layer with a thickness of around 7.5 mm is present from the top down to a depth of approximately 600 m. At 600–800 m, the thickness of the layer increases to 9.5 mm in the flashing zone. During this operation, it became evidenced that scale formation was occurring.

Under higher pressure conditions (Table 2), sulfide scaling, predominantly composed of galena (PbS), was observed close to the wellhead. In contrast, iron silicate (FeSiO_3) deposits were common at 2 to 16 bar/g, while amorphous silica (SiO_2) was the dominant constituent at lower pressures (Figure 4). The iron silicate (FeSiO_3) scale was characterized by a lean or

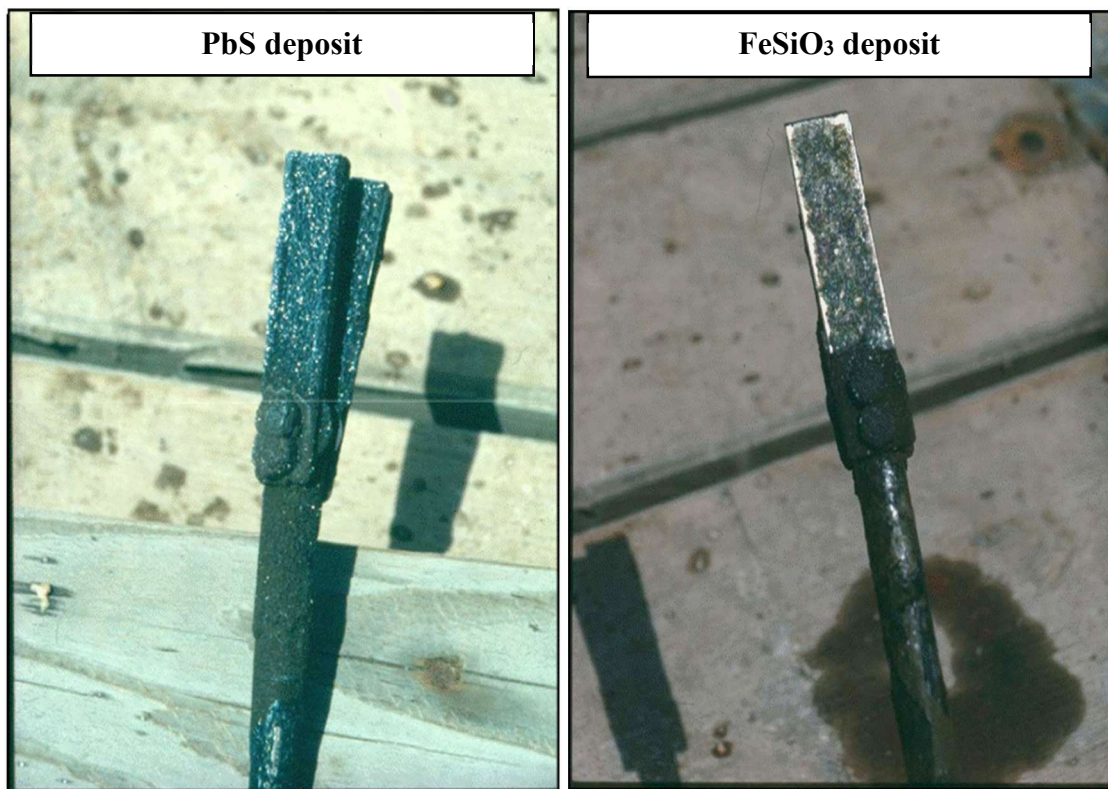


Figure 4: Sulfide (galena (PbS)) and iron silicate ($FeSiO_3$) on a deposition coupon (Armannsson et al., 1990)

uncrystallized yellow green poorly with significant amounts of Mn as well as sphalerite (zinc sulfide) crystals.

At the surface equipment, silica scaling predominated with traces of certain elements such as barium (Ba). In the critical lip pressures zones, traces of copper (Cu) have been observed (Virkir-Orkint, 1990). Chalcocite (CuS_2) has also been observed and has less well-characterized Fe and Mn products. Detailed chemical compositions of the scales at the Assal 3 wellhead are presented in Appendix A and the scaling rate of formation is shown in Figure 5. Two distinct types of inhibitors (Figure 6 a) were tested:

- Nadar 4093 (brown liquid): is a sequestering agent for heavy metals and designed to inhibit the iron silicate ($FeSiO_3$) scale. It is an aqueous solution of a mixture of aliphatic and aromatic polymers with simultaneous carbosilic and sulfonic functions associated with an amphoteric lactam derivative.
- Nadar 1008 (amber yellow liquid): Aqueous solution of carbosilic polymer, is a sequestering and dispersing agent against calcium (Ca), magnesium (Mg) salts and silica (SiO_2) respectively.

The results indicated the effectiveness of these inhibitors in preventing sulfide scaling. Nevertheless, a new form of scale, often referred to as pseudo-scale, appeared as a consequence of the chemical composition of the inhibitors, which incorporated elements like iron silicate and calcium into the inserted coupons (Figure 6b).

Table 2: The conditions at which scales formed in Assal 3 (Virkir-Orkint, 1990)

Scale	Chemical formula	P/T conditions	Location	Identified by	Inhibitors used
Sulfides	Galena (PbS), Sphalerite (ZnS), Chalcocite (CuS ₂)	>16 bar/g (>200°C)	Wellhead spool/ In the top of the casing	Optic microscopic	Nadar -4093 Nadar- 1008
Iron silicates	FeSiO ₃	2 to 16 bar/g (<200°C)	Silencer/ Pipes	X-ray fluorescence spectrometry/ X-ray diffraction	Keeping the wellhead (>16 bar/g)
Amorphous silica	SiO ₂	< 16 bar/g (<150°C)	Surface equipment/ Separator	Scanning Electron Microscopy (SEM)	Pseparator >Psaturation

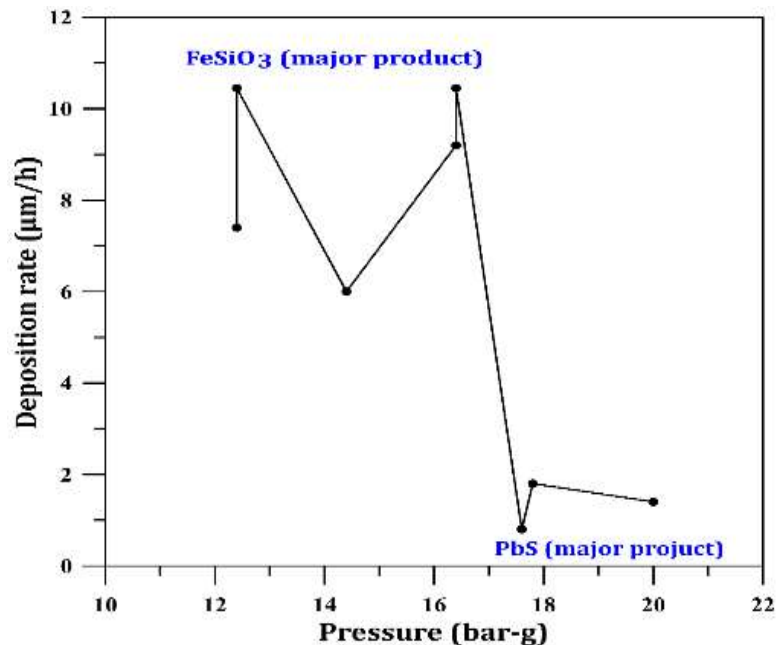


Figure 5: Scale deposition rate on coupons at different pressures of Assal 3. (modified from Virkir-Orkint, 1990)

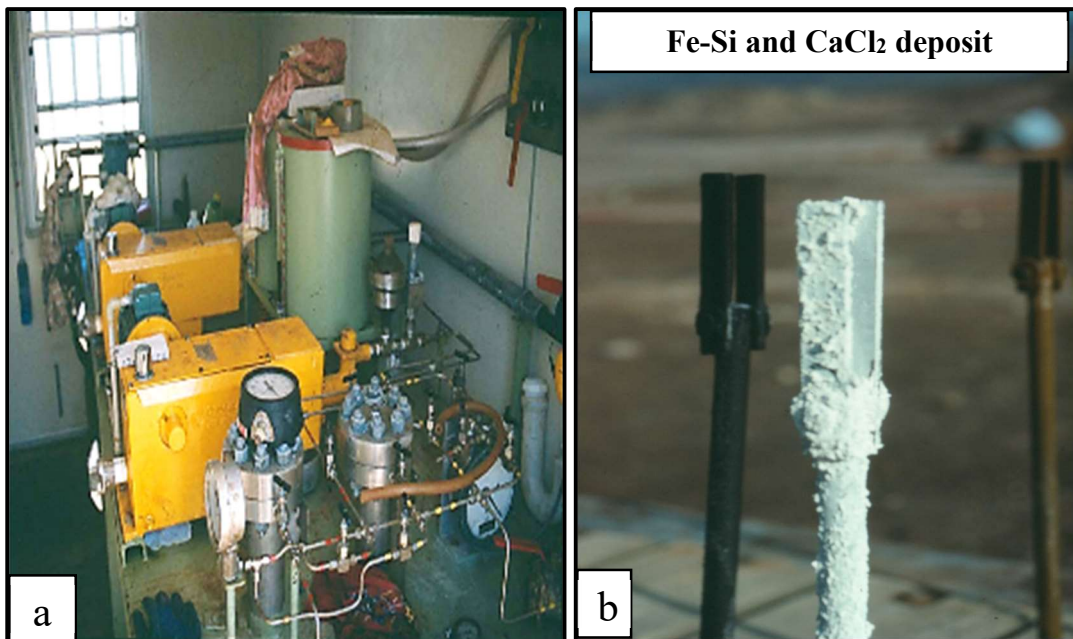


Figure 6: a) Dosage pumps for sulfide inhibitors; b) Iron silicates and calcium chloride pseudo scales on a deposition coupon (Ármansson et al., 1990).

3 Methods

3.1 Equipment

Sampling of the Assal 3 geothermal fluid was conducted during the testing of scale and corrosion potential carried out by Virkir-Orkint in 1990. The flow line primarily served to monitor the enthalpy, flow rates and to collect fluid samples at the beginning and end of the test, although it remained closed for most of the experiment. The components of the flow line comprised a Russel James lip pressure pipe, a twin cyclone atmospheric separator (silencer), and a weir box connected to the wellhead through a series of ten-inch gate valves and a ten-inch steel pipe. After the wellhead valves, it was placed an orifice plate for controlling the wellhead pressure.

The three side branches were responsible to bring two-phase fluid from the wellhead for the inhibitor test line, steam from the steam pipe for the corrosion assessment, and brine from the brine pipe (separator line). The separator line was composed of a two-phase line, a pressure separator (SE), a steam pipe, and a brine pipe that ultimately discharged into a silencer and a weir box. Coupons were strategically inserted into various locations along the inhibitor line, the separator line, and the brine pipe, among other points of interest (Figure 7).

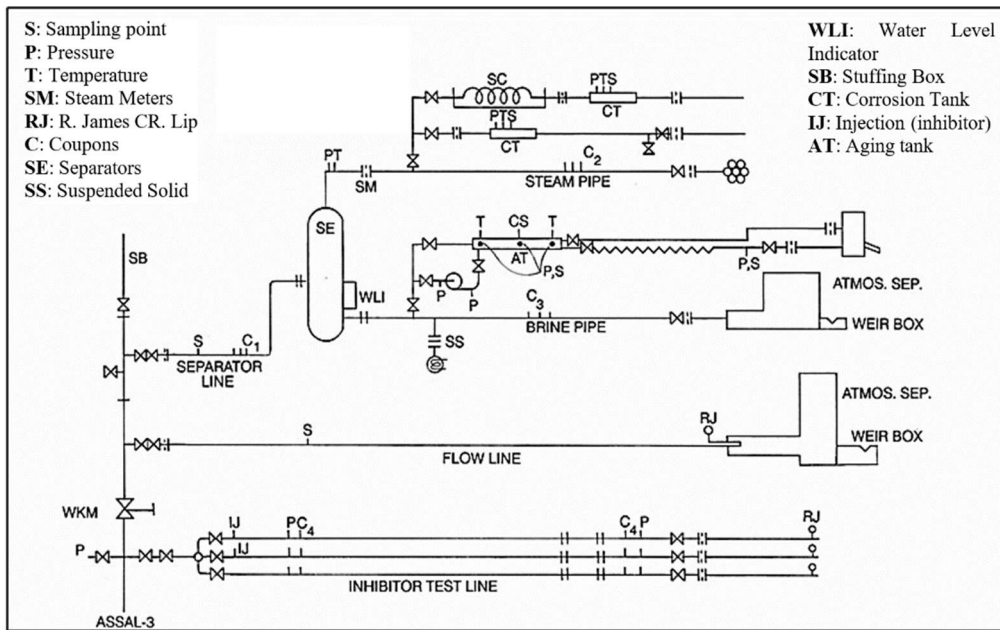


Figure 7: Equipment setup for testing scaling and corrosion on the Assal 3 modified from Virkir-Orkint, 1990.

Table 3: Analytical methods applied for studying of the fluids from Assal 3 well (Virikir-Orkint, 1990).

Constituent	General method	Special method	References
Hg	AAS	Gold amalgamation, flameless	Ólafsson (1994) Ármannsson (1981)
CO ₂	Titration	pH, glass electrode HgAc, dithizone	Ellis & Mahon (1977)
H ₂ S	Titration	indicator	Árnórsson (1969)
NH ₃	Spectrophotometry	Indophenol blue	Koroleff (1981)
CO ₂	Gas chromatography		Hauksson (1981)
H ₂ S	Gas chromatography		
CH ₄	Gas chromatography	Poropak, Molecular sieve	
H ₂ , N ₂	Gas chromatography		
O ₂ , CO ₂	Gas chromatography		
C ₂ ⁺	Gas chromatography		
pH	Electrode Bridge	Glass	
Conductivity			
SiO ₂	Spectrophotometry	Ammonium molybdate	APHA (1985), Elisson (1969) Grinstead & Snider (1967)
B	Spectrophotometry	Curcumin	
Cl, Br, F	Ion chromatography		
Cl	Titration	AgNO ₃	ASTM (1966)
SO ₄	Ion chromatography		
Na	AAS	Li added, flame	Ármannsson & Hauksson (1978)
K, Li	AAS	Flame	
Ca, Mg	AAS	La added, flame	Willis (1961)
Sr			
Fe	Spectrophotometry AAS	TPTZ Flame	Koroleff (1983 b)
Mn	Spectrophotometry	Formaloxime	Koroleff (1983 c)
Al	Fluorimetry ICP	Lumogallion	Hydes & Liss (1976) Moore (1989)
Zn	AAS	Flame	
Cd, Cu			
Ni, Pb	AAS	Flameless	
Ag			
Ba	ICP		Moore (1989)

3.2 Sampling and analysis

Two fluid samples were collected from the wellhead, with the first samples collected on January 11 and the second on January 30, both in 1990. An additional sample was gathered from the flow line on March 12, 1990. For the collection of two-phase fluid samples, a small Weber separator was employed.

The liquid samples were classified according to the specific constituent to be analysed afterwards: raw, filtered, untreated, acidified, precipitated, and extracted. In the case of steam samples, collection was performed using Giggenbach bottles containing a solution of NaOH, in order to determine the soluble gases (CO₂, H₂S) by titration and the non-condensable gases (H₂, O₂, CH₄, N₂) using gas chromatography.

The analysis of the discharged fluids included various parameters and elements, with pH and conductivity being determined via electrometry. Atomic Absorption Spectroscopy (AAS) was employed to analyse the concentrations of Na, K, Li, Ca, Mg, Sr, Fe, Zn, Cd, Hg, Cu, Ni, Pb, and Ag. Additional constituents such as NH₃, SiO₂, B, Fe, and Mn were quantified by UV/Vis Spectrophotometry. Aluminium (Al) was determined using fluorimetry and ICP, while barium (Ba) concentrations were assessed via ICP/AES. The concentrations of CO₂ and H₂S were determined by titrations and Cl, Br, F, and SO₄ were quantified using ion chromatography (IC). A summary of the analytical methods is presented in Table 3.

3.3 Data analysis

3.3.1 Reservoir fluid composition

In this thesis, the chemical composition of the liquid and gas samples have been utilized to calculate the deep reservoir fluid composition. The chemical species and component concentration of discharged fluid were calculated using the WATCH speciation programme version 2.4 (Bjarnason, 2010).

The speciation calculations were conducted assuming an isolated system in which neither heat nor mass is transferred from the reservoir to the surface. The three samples collected were used to determine the reservoir fluid composition. The selected reference temperatures used for the calculations were based on the quartz geothermometer and ranged from 245°C to 251 °C. The equations to calculate the deep fluid composition are described in the equation (1) and (2) as follow:

$$m_i^{f,t} = m_i^{d,t} = X^{d,v} m_i^{d,t} + (1 - X^{d,v}) m_i^{d,lq} \quad (1)$$

$$h^{f,t} = h^{d,t} = X^{d,v} h^{d,v} + (1 - X^{d,v}) h^{d,lq} \quad (2)$$

Where m_i stands for the concentration of the dissolved component of i , X is the vapour fraction of the well fluid discharge, h is the enthalpy of the fluid and f , t , d , v , and lq represent the fluid, total, discharge, vapor, and liquid phase respectively.

3.3.2 Mineral saturation

The aqueous speciation and mineral saturation indices of the calculated reservoir fluid were calculated using the PHREEQC program (Parkhurst and Apello, 1999). The llnl.dat database was selected as the thermodynamic database which includes metal-bearing minerals. The input data was the composition of the deep fluid calculated using the WATCH program and the reference temperature.

The mineral saturation index (SI), which is calculated as the logarithm of the reaction quotient (Q) divided by the logarithm of the equilibrium constant (K) (see equation 3), can be used to determine the mineral saturation state in a solution and to predict its potential for dissolution or precipitation. Both parameters are temperature dependent.

$$SI = \log (Q/K) \quad (3)$$

- SI > 0, the solution is supersaturated, and the mineral may form.
- SI < 0, the solution is undersaturated and the mineral may dissolve.
- SI = 0, the solution is at equilibrium and the mineral are stable.

The effects of cooling and boiling on fluid composition and mineral saturation were modelled using WATCH and PHREEQC programs. The equations used for this modelling are presented in Appendix B.

4 Results and Discussion

4.1 Surface fluid compositions

The chemical analysis results for the three discharge samples collected from Assal 3 and the compositions of samples from the Ghoubbet seawater and from Lake Assal are detailed in Table 4. Specifically, samples A3_1 and A3_2 was collected from the wellhead, while sample (A3_3) was taken from the separator line using a small Weber separator during the scale and corrosion tests conducted in 1990.

The chloride concentrations of the discharged fluid ranged from 76,400 to 81,400 mg/kg and are 3 to 4 times higher than the chloride concentration of Ghoubbet seawater (21,059 mg/kg). In contrast, lower concentrations of Mg and SO₄, 21.4 to 24.2 and 8 to 14 mg/kg respectively were found in the discharged fluid. Comparatively, both seawater and Lake Assal shown significantly higher levels of Mg, with 1,397 mg/kg and 12,700 mg/kg, and SO₄, with 2,633 mg/kg and 2,576 mg/kg, respectively.

On the other hand, the concentrations of SiO₂, K, and Ca in the discharged fluid were notably higher, ranging from 490 to 521 mg/kg, 5,010 to 5,335 mg/kg, and 17,030 to 18,250 mg/kg, respectively. These concentrations exceeded the corresponding levels in both seawater and Lake Assal waters.

Table 4: Chemical compositions of the fluids discharged from well Assal 3, Ghoubbet seawater and Lake Assal (Virkir-Orkint, 1990).

Sample N°	A3_1 (WH)	A3_2 (WH)	A3_3 (Flow line)	Ghoubbet (seawater)	Lake Assal
Date	11-01-90	30-01-90	12-03-90	-	28-11-2017
H (kJ/kg)	1,069	1,069	1,080	-	-
Cond (S/cm)	129,900	116,500	108,000	-	-
Cond. temp (°C)	23.3	31.5	39.0	-	-
P (bar-g)	19.4	19.2	16.4	-	-
T (°C)	-	-	-	-	32.2
Liquid (ppm)					
pH	5.40	5.20	3.94	-	6.92
pH temp (°C)	26.7	31.5	39.0	-	22.1
SiO ₂	521.3	494.1	490	1.2	13.7
Na	30,000	28,400	31,450	11,426	100,700
K	5,045	5,010	5,335	438	5,180
Ca	17,035	17,030	18,250	409	2,810
Mg	24.4	21.4	24.4	1,398	12,700

CO ₂	253.7	230	578	-	258
HCO ₃	-	-	-	-	-
SO ₄	14	8	10	2,633	2576
H ₂ S	<0.1	<0.1	0	-	-
Cl	80,450	76,400	81,400	21,059	196,800
F	5.5	9.5	10.3	-	0.27
TDS	131,856	130,240	139,388	-	-
Al	1.7	3.4	2	-	-
B	10.3	9.8	9.2	4.8	47.7
Fe	36.6	35.0	32.8	-	-
Br	-	-	-	80.8	723
NH ₃	6.4	5.4	5.9	-	-
Sr	339	168	190	8.4	-
Br	183	310	331	-	-
Mn	131	123	142	-	-
Zn	41.9	40.0	41.0	-	-
Pb	1.4	1.12	1.15	-	-
Cu	0.31	<0.1	<0.1	-	-
Ag	<0.001	<0.001	<0.001	-	-
Cd	0.01	<0.01	0.01	-	-
Li	15.6	14.9	15.6	-	-
Ba	93.0	68.5	-	-	-
Ni	<0.1	<0.1	<0.1	-	-
Hg (ng/l)	23.0	42.0	51.7	-	-
Gas (vol. %)					
CO ₂	98.33	98.5	98.41	-	-
H ₂ S	0.27	0.19	0.26	-	-
H ₂	0.24	0.24	0.21	-	-
O ₂	0.05	0.02	0.05	-	-
CH ₄	0.08	0.09	0.10	-	-
N ₂	1.03	0.96	0.97	-	-
Condensate					
pH/T°C	4.28/24	4.64/26.3	4.94/36.2	-	-
CO ₂	932.6	1063	910.4	-	-
H ₂ S	5.3	3.3	4.8	-	-
Na	0	1.5	1.97	-	-

- - Not measured

- **WH:** wellhead samples from Virkir-Orkint (1990)

- **Flow line:** sample from separator line by Virkir-Orkint (1990)

- **Ghoubbet** (seawater) from Sanjuan *et al.* (1990)

- **Lake Assal** from Thorbjörnsson *et al.* (2017)

4.2 Deep fluid composition

The chemical composition of the deep fluid was calculated at the quartz geothermometer. The results of these calculations are presented in Table 5. As can be seen the reservoir temperature ranges between 245 and 251 °C, and pH between 4.4 and 5.2. The chloride concentration ranges between 69,926 mg/kg and 73,587 mg/kg which is 3 to 4 times higher than that of the Ghoubbet seawater (20,846 mg/kg). These waters can be classified as sodium-chloride type with relatively low content of CO₂ (256-318 ppm) and H₂S (0.3-0.5 ppm) in comparison to another geothermal fluid (Table 7).

Table 5: Deep aquifer fluid compositions of Assal geothermal wells. (Concentrations are given in mg/kg).

Sample n°	Assal 3			Ghoubbet seawater	Lake Assal
	A3_1	A3_2	A3_3		
T _{qtz} °C	251	251	245	-	32.2
H ^{dt} (kJ/kg)	1069	1069	1080	-	-
H ^{d,l} (kJ/kg)	1092	1071	1080	-	-
Pd (bar.abs)	20.4	20.2	17.4	-	-
pH	5.2	5.0	4.4	-	-
X	0.09	0.1	0.105	-	-
B	9.3	9.0	8.3		47.7
SiO ₂	472	452	443	1.2	13.7
Na	27,154	25,993	28,431	11,426	100,700
K	4,566	4,585	4,823	438	5,180
Mg	22.1	19.6	22.1	1397	12,700
Ca	15,419	15,587	16,498	409	2,810
F	5.0	8.7	9.3	-	0.27
Cl	72,818	69,926	73,588	21,059	196.8
SO ₄	12.7	7.32	9.0	2633	2576
Al	1.5	3.1	1.8	-	-
Fe	33.1	32.0	29.7	-	-
CO ₂	318	301	256	-	-
H ₂ S	0.5	0.3	0.3	-	-
NH ₃	5.8	4.9	5.3	-	-
TDS	119,348	119,203	126,010	-	-
Sr	307	154	170	8.4	
Br	166	284	296	80.8	723
Mn	119	113	127	-	-
Zn	37.9	36.6	36.7	-	-
Pb	1.3	1.0	1.0	-	-
Cd	0.01	-	0.01	-	-
Li	14.1	13.6	13.9	-	-
Ba	84.2	62.7		4.9	-
Hg	20.8	38.4	46.2	-	-

4.3 Mineral saturation

The selection of minerals for further modelling analysis have been conceived based on the chemical composition of both scales observed in the field and the lithology of the area, and the thermodynamic database available. The following chapters will provide a comprehensive assessment of the behaviour of silica, sulfate, sulfide, carbonate, and oxide minerals in various scenarios involving both boiling and cooling processes. Depressurization during the fluid ascent to the surface results in boiling and therefore separation of a vapor phase, primarily composed of H₂O and notable concentrations of H₂S and CO₂. During this process the boiled liquid becomes enriched in non-volatile substances. Additionally, conductive cooling and mixing with sub-boiling water may also occur.

4.3.1 Silica and silicate mineral saturation

The saturation index of silica and silicate minerals, including ferrosilite (Fe₂Si₂O₆) in this section, was conducted. The results reveal a similar pattern under boiling and cooling conditions, except for ferrosilite (Figure 8). At temperatures between 230°C and 185°C, the reservoir fluid of Assal 3 becomes undersaturated with cristobalite alpha and beta, respectively, while remaining supersaturated or close to equilibrium with respect to quartz and chalcedony minerals. The concentration of silica is controlled by the solubility of quartz in geothermal systems at 200-350°C, and it increase at higher temperatures (Gunnlaugsson, 2012; Fournier and Rowe, 1966; and Mahon, 1966).

Nevertheless, amorphous silica supersaturation occurs in the fluid at temperatures between 150 °C and 125 °C (surface conditions). In comparison to other silica forms, amorphous silica precipitates at low temperatures much more quickly and is the dominant deposition in surface equipment as well as where wastewater is discharged (Tassew, 2001; van den Heuvel et al., 2018 and references therein).

The boiling model states that the iron silica (ferrosilite) mineral becomes oversaturated as it rises from the reservoir condition to the surface on the wellhead samples. Nonetheless, the flowline fluid samples are undersaturated with the respect to the ferrosilite mineral. This can be due to the lower pH in this sample as shown in figure 10. As the adiabatic boiling and conductive cooling proceed and the water temperature is lowered, the activity of the iron hydroxide complex is reduced as plotted in Fe (OH)₄⁻ activity versus the aquifer fluid temperature in figure 9. According to Stefán and Sven (1982), the rise in pH accompanying boiling will decrease the concentration of Fe²⁺ in the solution by forming hydroxide complexes. Which means that the iron content is in co-dependency of pH. This mineral has been identified within the surface scales.

The results indicate that silica scales tend to develop at surface conditions under the boiling and cooling scenarios. This observation confirms that at lower pressures, silica scales become the predominant deposit (Table 6). The concentration of silica increases and precipitates when the temperature decreases, typically occurring at pH values lower than 8.5 (Dove and Rimstidt, 1994). Silica scale deposition from geothermal fluids can take place over intervals of minutes or hours after supersaturation (Tassew, 2001).

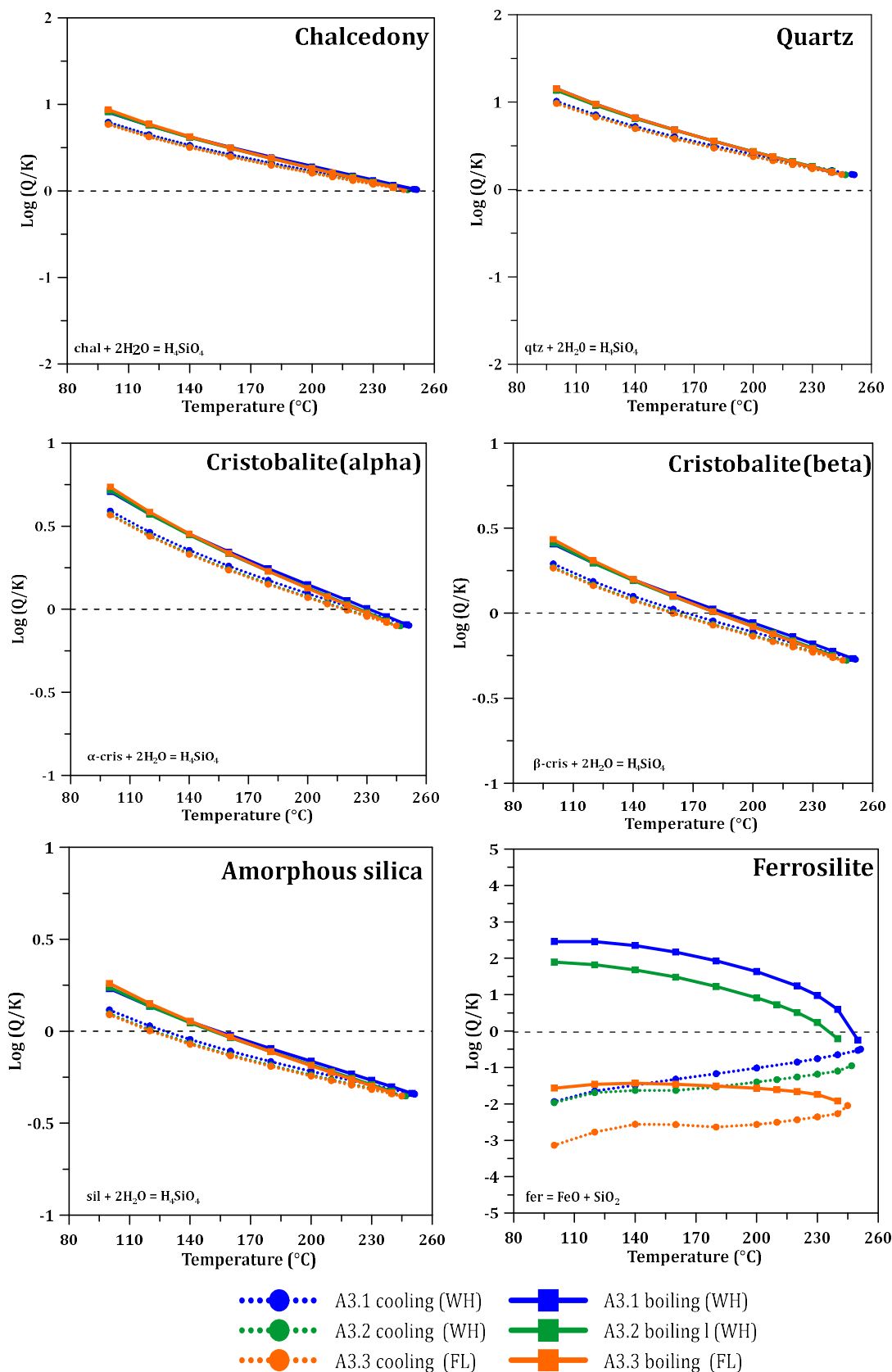


Figure 8: Saturation state with respect to silica minerals upon boiling (solid line) and cooling (dotted line).

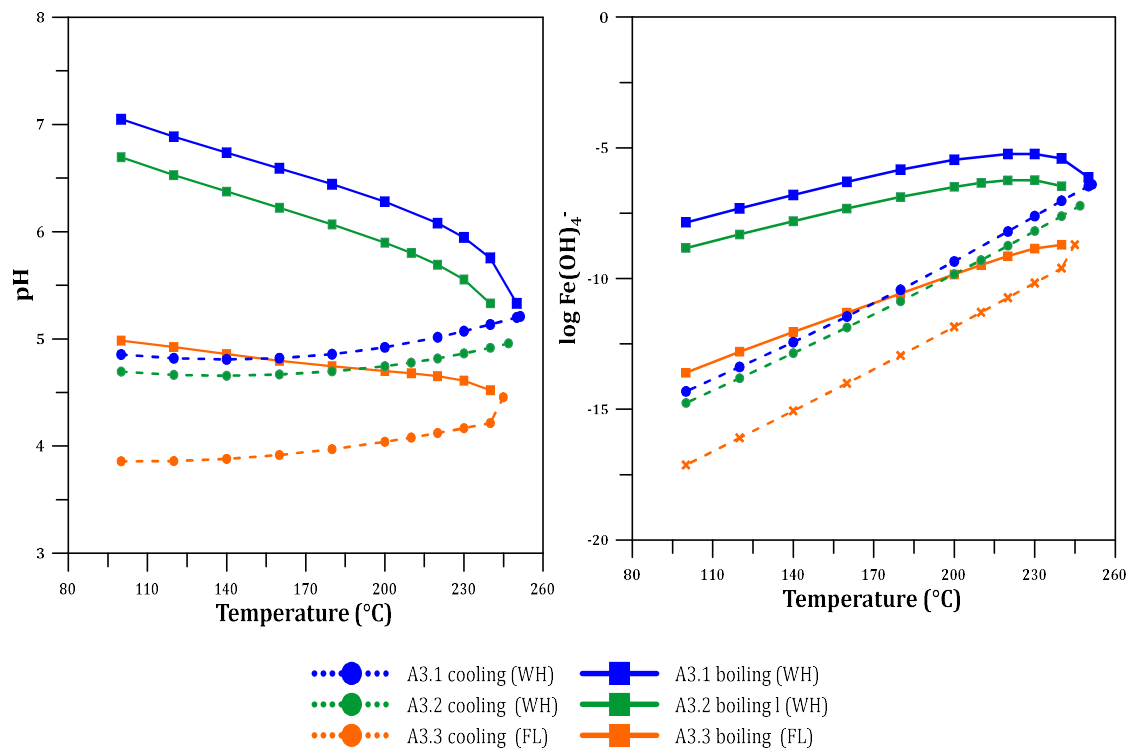


Figure 9: pH and $Fe(OH)_4^-$ activity ratios plots versus aquifer temperature

4.3.2 Sulfate mineral saturation

According to the sulfate minerals saturation index (Figure 0), anhydrite ($CaSO_4$) approaches the equilibrium in the reservoir under boiling conditions and temperatures higher than $200^\circ C$, and it becomes undersaturated in the cooling model. Additionally, under both boiling and cooling conditions, the fluid is undersaturated with respect to gypsum ($CaSO_4 \cdot 2H_2O$) and alunite ($KAl_3(SO_4)_2(OH)_6$).

The results indicate that under boiling conditions, there is potential for the precipitation of sulfate minerals in the form of anhydrite. This observation suggests that sulfate minerals may not precipitated at the surface.

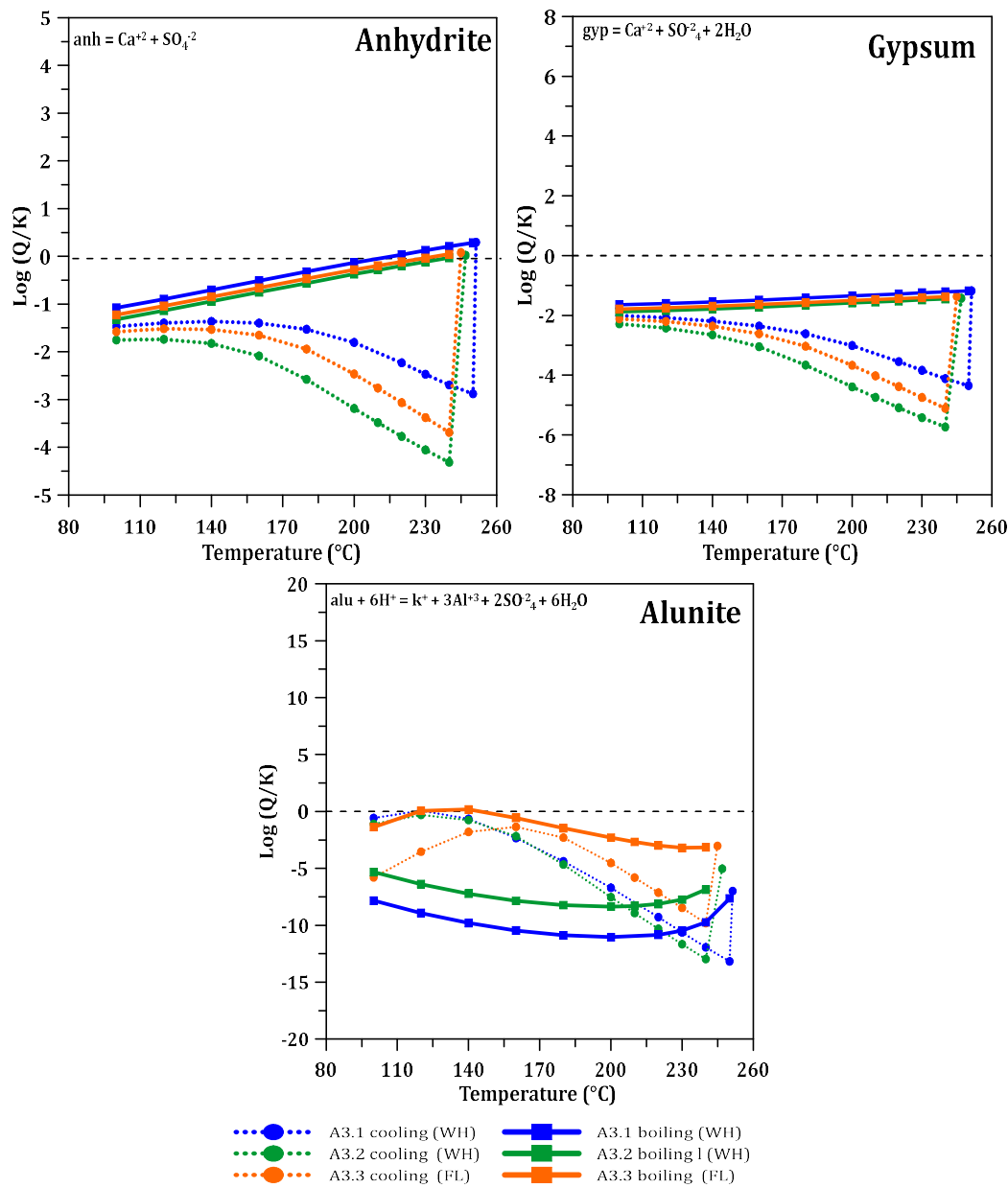


Figure 10: Saturation state with respect to sulfate minerals upon boiling (solid line) and cooling (dotted line).

4.3.3 Sulfide mineral saturation

The sulfide saturation indices reveal a considerable difference between the calculations under boiling and cooling models (Figure 11). Galena (PbS) is supersaturated at lower temperature, and it approaches the equilibrium at temperatures ranging from 200°C to 150°C in the cooling model. Sphalerite ((Zn,Fe)S) is close to the equilibrium at the reservoir temperature, and it becomes supersaturated when the temperature decreases during cooling.

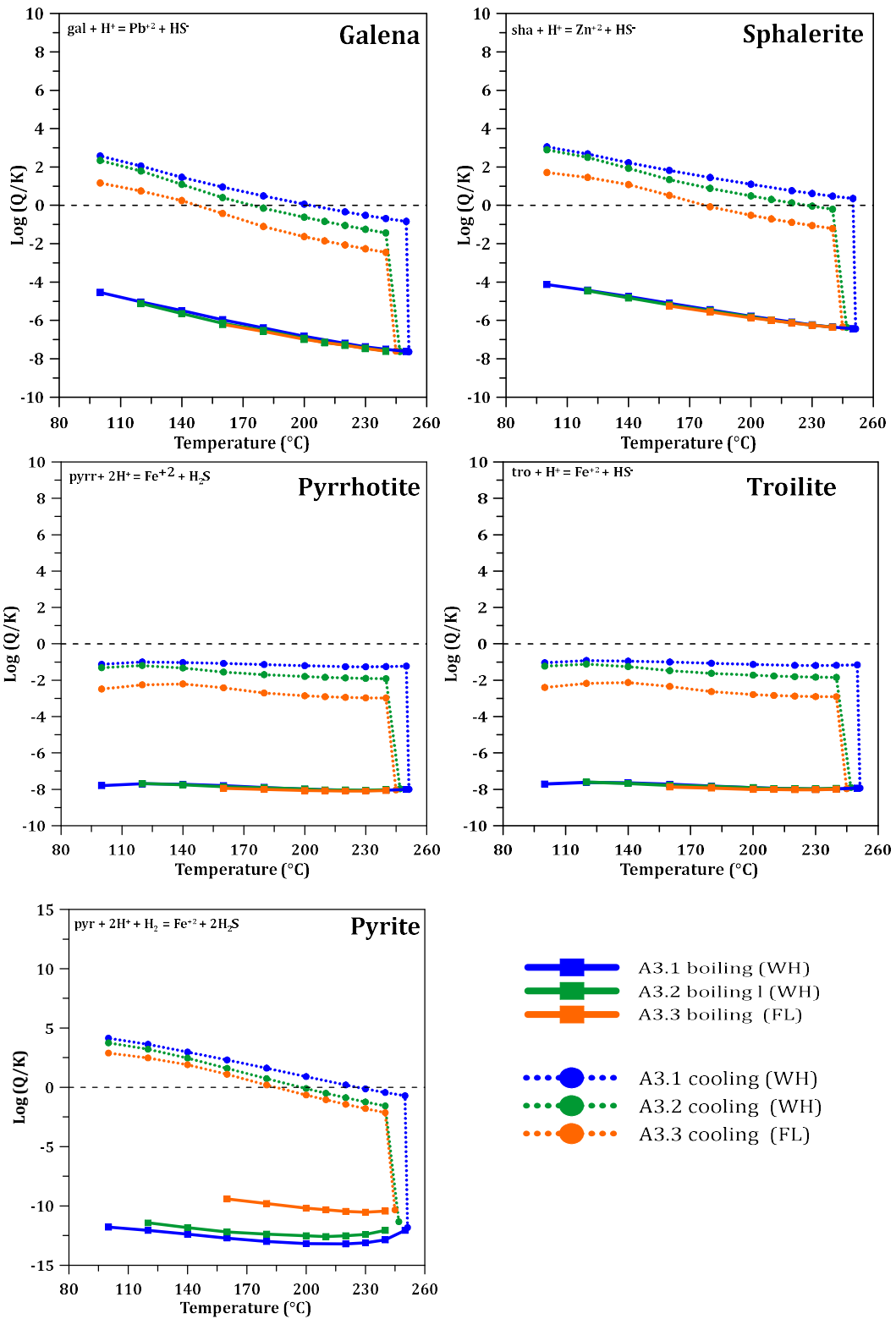


Figure 11: Saturation state with respect to sulfide minerals upon boiling (solid line) and cooling (dotted line).

Pyrite (FeS_2) is undersaturated at the reservoir conditions in the cooling model and precipitates at temperature lower than 230°C . On the other hand, the boiling and cooling model predicts that the aquifer fluid is undersaturated with respect pyrrhotite (FeS) and troilite (FeS).

At relatively low temperatures ($<170^\circ\text{C}$), galena, sphalerite, and pyrite tend to precipitate in the cooling model, which is in agreement with the results of the scaling tests performed by Virkir-Orkint (1990). This observation suggests that the cooling model may offer good predictions regarding mineral formations despite boiling happening within the borehole. Moreover, boiling releases CO_2 from the liquid phase, which raises pH and decreases sulfide mineral solubility while destabilising chloride complexes. On the other hand, H_2S loss promotes the precipitation of metals carried by sulfide complexes (Hardardóttir et al. 2005). The high decrease in SI calculated at the onset of the cooling model is due to equilibration of pe and pH at the calculated temperature intervals resulting in adjusting of these parameters significantly affecting the model outcome.

4.3.4 Carbonate Mineral saturation

Considering the boiling model shown in Figure 12, calcite (CaCO_3) is close to equilibrium at the reservoir temperature, but it becomes oversaturated at temperatures below 200°C for the WHP samples. On the other hand, the calculations show that calcite is always undersaturated according to the cooling model.

Considering both the boiling and cooling model, siderite (FeCO_3) is undersaturated between the reservoir and surface temperature. According to the boiling model, the aquifer fluid becomes saturated with respect to dolomite ($\text{CaMg}(\text{CO}_3)_2$) at 230°C and with respect to aragonite (CaCO_3) at 245°C .

The results demonstrate the formation of calcite, dolomite, and aragonite in the Assal 3 well. However, the degassing of carbon dioxide (CO_2) and the rise of pH may have influenced the carbonate mineral precipitation. According to Houmed *et al.*, (2012) and Battistelli et al. (1991), carbonate scale can be present downhole, most likely just above the flashing zone, where partial pressure of CO_2 is quickly decreasing rapidly as the flashing process proceeds. The major mineral found in one scale sample that may be representative of scaling products downhole is calcite (Table 6), according to an x-ray examination by Battistelli, et al. (1991).

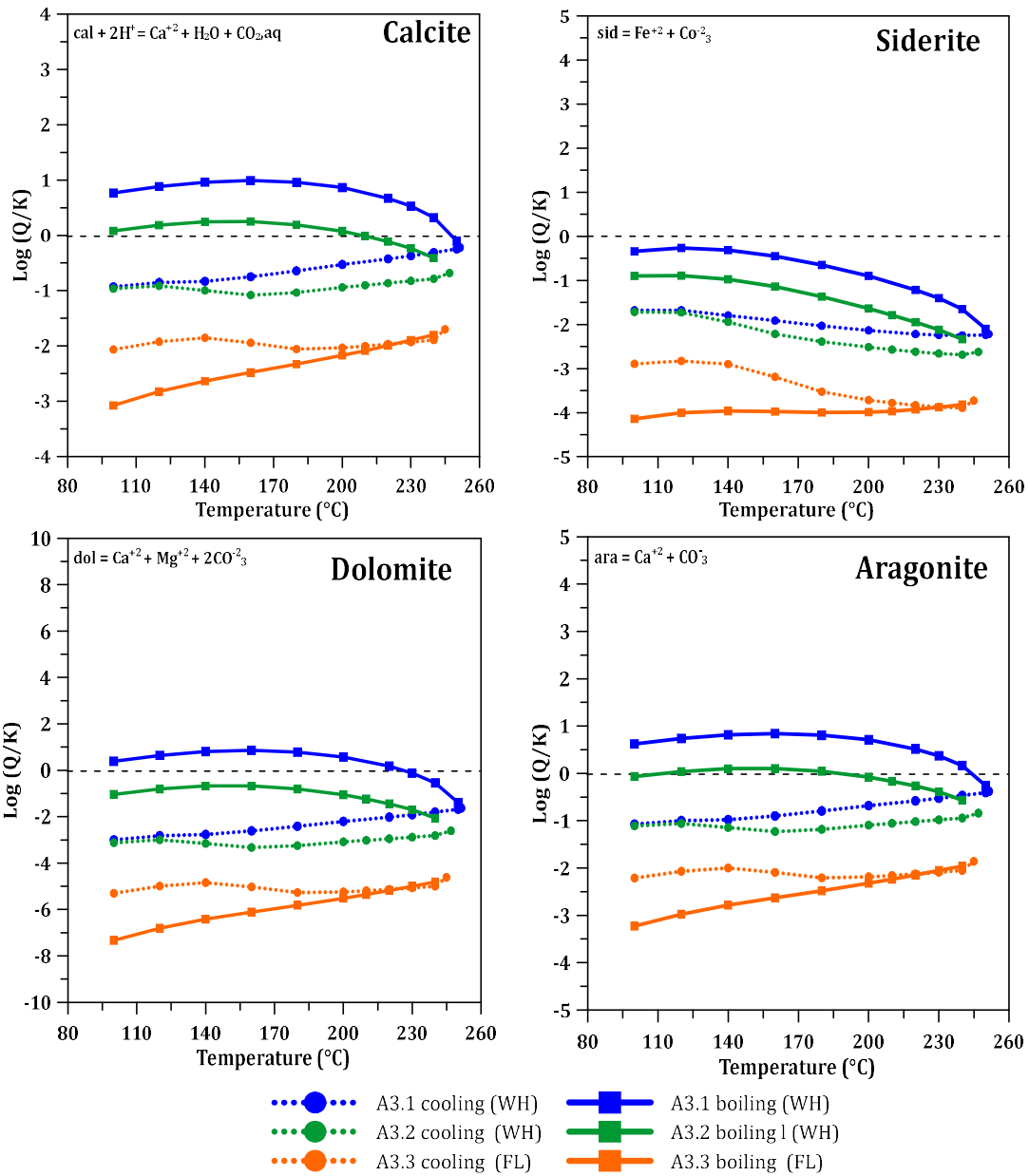


Figure 12: Saturation state with respect to carbonate minerals upon boiling (solid line) and cooling (dotted line).

4.3.5 Oxide Minerals saturation

The saturation index in function of temperature for goethite (FeO_2H), magnetite (Fe_3O_4) and hematite (Fe_2O_3) are presented in Figure . In the case of each of these minerals, both the boiling and cooling models were considered for the calculations.

There is a significant discrepancy between these models since the boiling model predicts consistently supersaturation at all stages, the cooling model indicated undersaturation for all

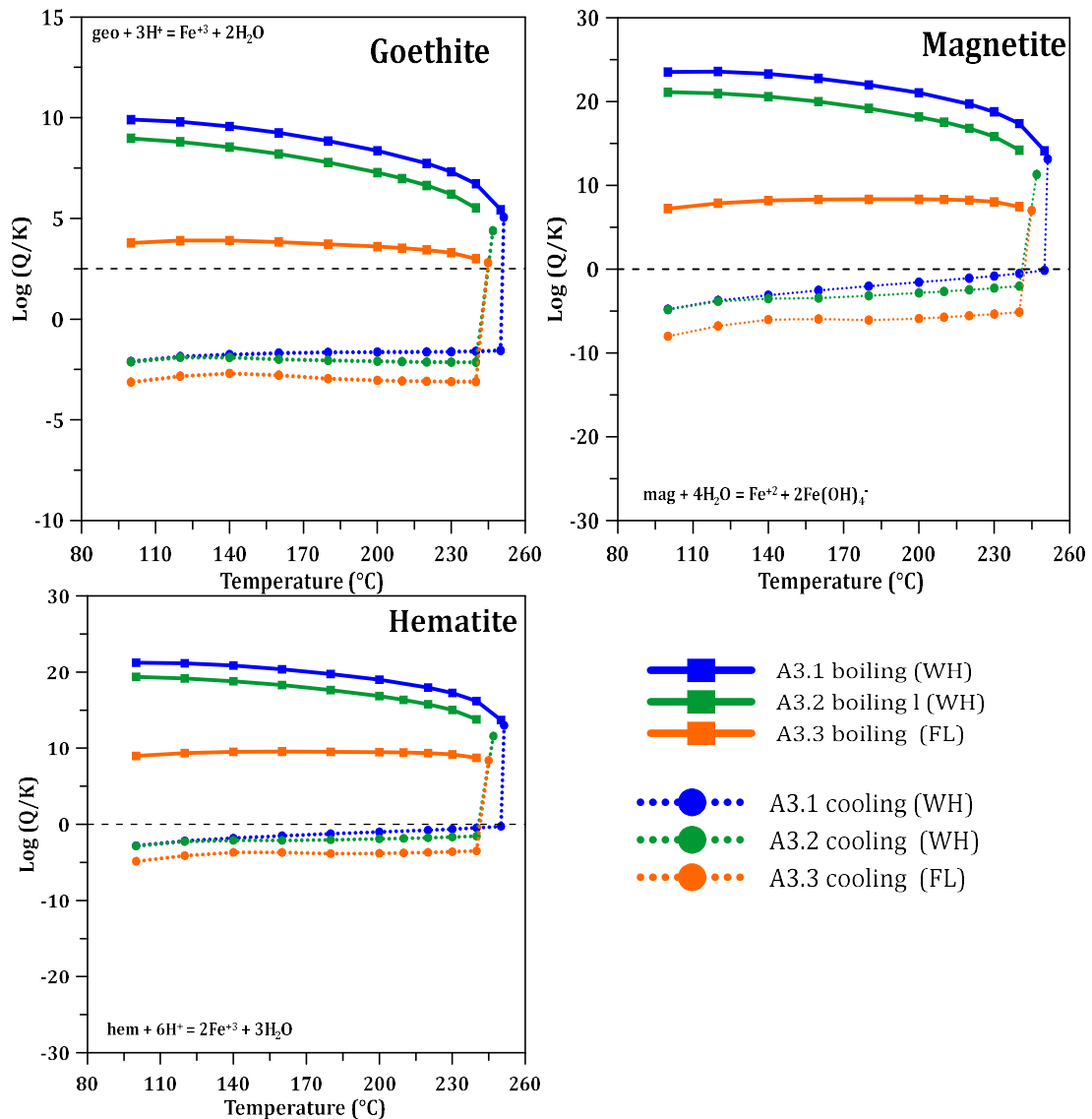


Figure 13: Saturation state with respect to oxide minerals upon boiling (solid line) and cooling (dotted line).

the given temperatures. Since no oxide scales were observed during the scale test conducted in 1990 (Virkir-Orkit), it seems that the cooling model offers a more accurate representation of the fluid's behaviour during its ascent to the surface. Note, however, that this is not the process that is observed in the borehole. The disagreement might be related to the inaccurate representation of the discharged fluid in terms of trace metals concentrations and due to inconsistencies in the thermodynamic databases used in the calculations.

4.3.6 Other mineral saturation

The deep fluid in the well Assal 3 is oversaturated with respect to the low albite ($\text{NaAlSi}_3\text{O}_8$), epidote ($\text{Al}_2\text{FeSi}_3\text{O}_{12}(\text{OH})$), and illite ($\text{K}_6\text{Mg}_{25}\text{Al}_6\text{Si}_{15}\text{O}_{10}(\text{OH})_2$) (Figure). Both the boiling and cooling models predict similar behaviour for low-albite and illite, which has not been observed in the scale samples but in the lithology of the area.

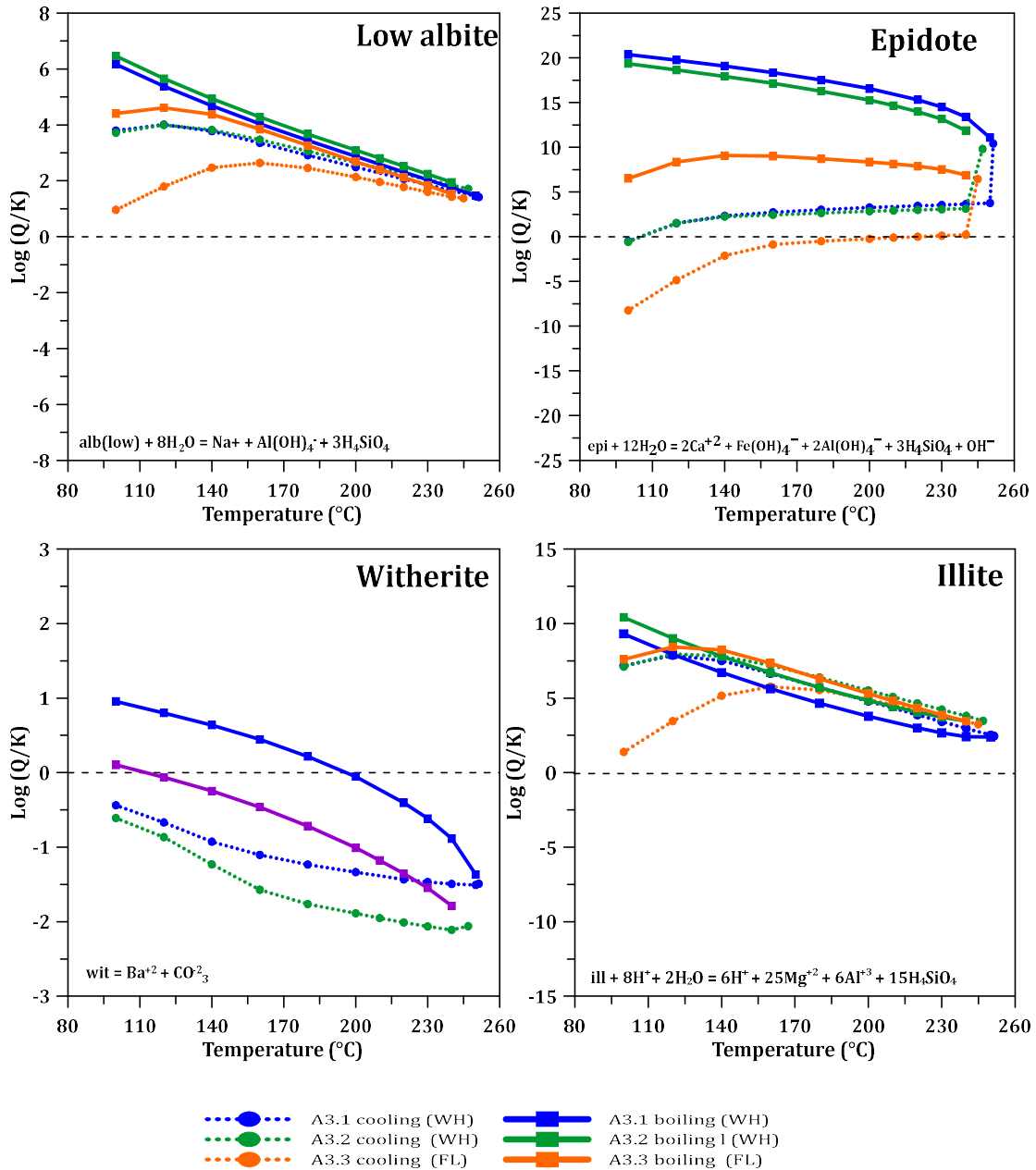


Figure 14: Saturation state with respect to epidote, low albite, witherite and illite minerals upon boiling (solid line) and cooling (dotted line).

The summary of scales observed, lithology and the saturation index calculated for the models are presented in Table 6. Figure 1515 shows a summary of Saturation indices (SI) with respect to silica, sulfide, sulfate, carbonate, oxide and other calculated from Assal aquifer fluid upon adiabatic boiling (red colour) and cooling model (green colours).

Table 6: Comparison between model and field observations regarding the scales.

	Mineral	Formula	Scale observed	Cooling model	Boiling model	Lithology
Silica	Quartz	SiO ₂		✓	✓	✓
	Chalcedony	SiO ₂		✓	✓	✓
	Cristobalite (alpha)	SiO ₂		✓	✓	
	Cristobalite (beta)	SiO ₂		✓	✓	
	Amorphous silica	SiO ₂	✓	✓	✓	
	Ferrosilite	FeSiO ₃	✓		✓	
Sulfide	Galena	PbS	✓	✓		
	Sphalerite	(Zn,Fe)S	✓	✓		
	Chalcocite	CuS ₂	✓			
	Pyrite	FeS ₂		✓		✓
	Pyrrhotite	FeS				
	Troilite	FeS				
Sulfate	Anhydrite	CaSO ₄				
	Gypsum	CaSO ₄				
	Alunite	KAl ₃ (OH) ₆ (SO ₄) ₂				
Carbonate	Calcite	CaCO ₃	✓		✓	✓
	Siderite	FeCO ₃				
	Dolomite	CaMg(CO ₃) ₂			✓	
	Aragonite	CaCO ₃			✓	
Oxide	Goethite	FeO (OH)			✓	
	Magnetite	Fe ₃ O ₄			✓	
	Hematite	Fe ₂ O ₃			✓	
Others	Epidote	Al ₂ FeSi ₃ O ₁₂ (OH)		✓	✓	✓
	Low albite	NaAlSi ₃ O ₈		✓	✓	✓
	Witherite	BaCO ₃			✓	
	Illite	K ₆ Mg ₂₅ Al ₆ S ₁₅ O ₁₀ (OH) ₂		✓	✓	✓

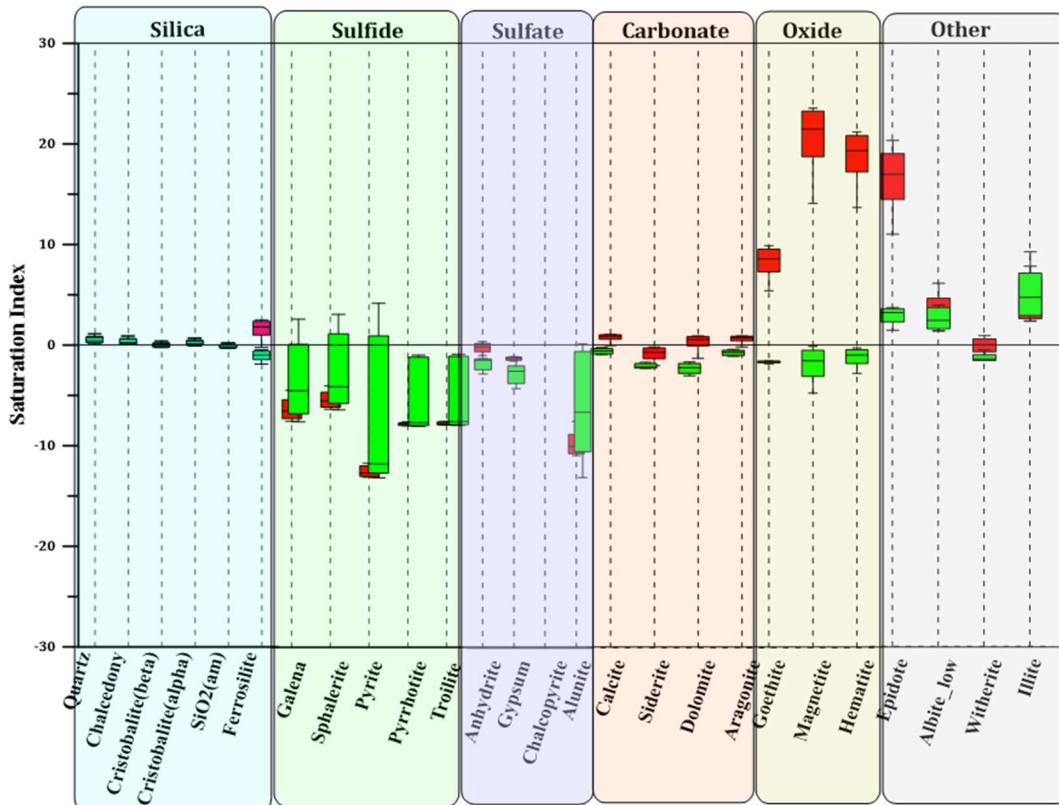


Figure 15: Saturation indices (SI) with respect to silica, sulfide, sulfate, carbonate, oxide and other calculated from Assal aquifer fluid upon adiabatic boiling (red colour) and cooling model (green colours)

4.4 Trace elements

Based on the research conducted by Virkir-Orkint in 1990, it was determined that trace elements such as Fe, Mn, Zn, and Pb are potential scaling agents due to their elevated concentrations in the fluids of the well Assal 3. The saturation index of minerals containing these trace elements are presented in (Figure 8).

The saturation calculations for sulfide minerals, including galena, sphalerite, alabandite, and pyrite, were modelled under cooling conditions as explained in before the cooling model describes better the behaviour of sulfide saturation minerals in the aquifer fluid. While the boiling model was applied for the remaining minerals. The sulfide minerals, in general, tend to become supersaturated in the temperature range of 230°C to 200°C, possibly attributed to the higher concentration of Fe in the fluid.

Carbonate minerals, except for siderite, are typically undersaturated, except siderite which gets closer to the equilibrium line at lower temperatures. Manganite and zincite, are found to be undersaturated, whereas goethite tend to be supersaturated. Rhodonite, a Mn-silicate

mineral, tends to become supersaturated or closely approach equilibrium around temperature of 200°C. Silica minerals, such as ferrosilite, exhibit supersaturation with respect to Fe in the aquifer fluid. In summary, the results indicate that most scale-forming minerals tend to accumulate higher concentrations of the iron, possibly due to interactions with the basaltic reservoir rock.

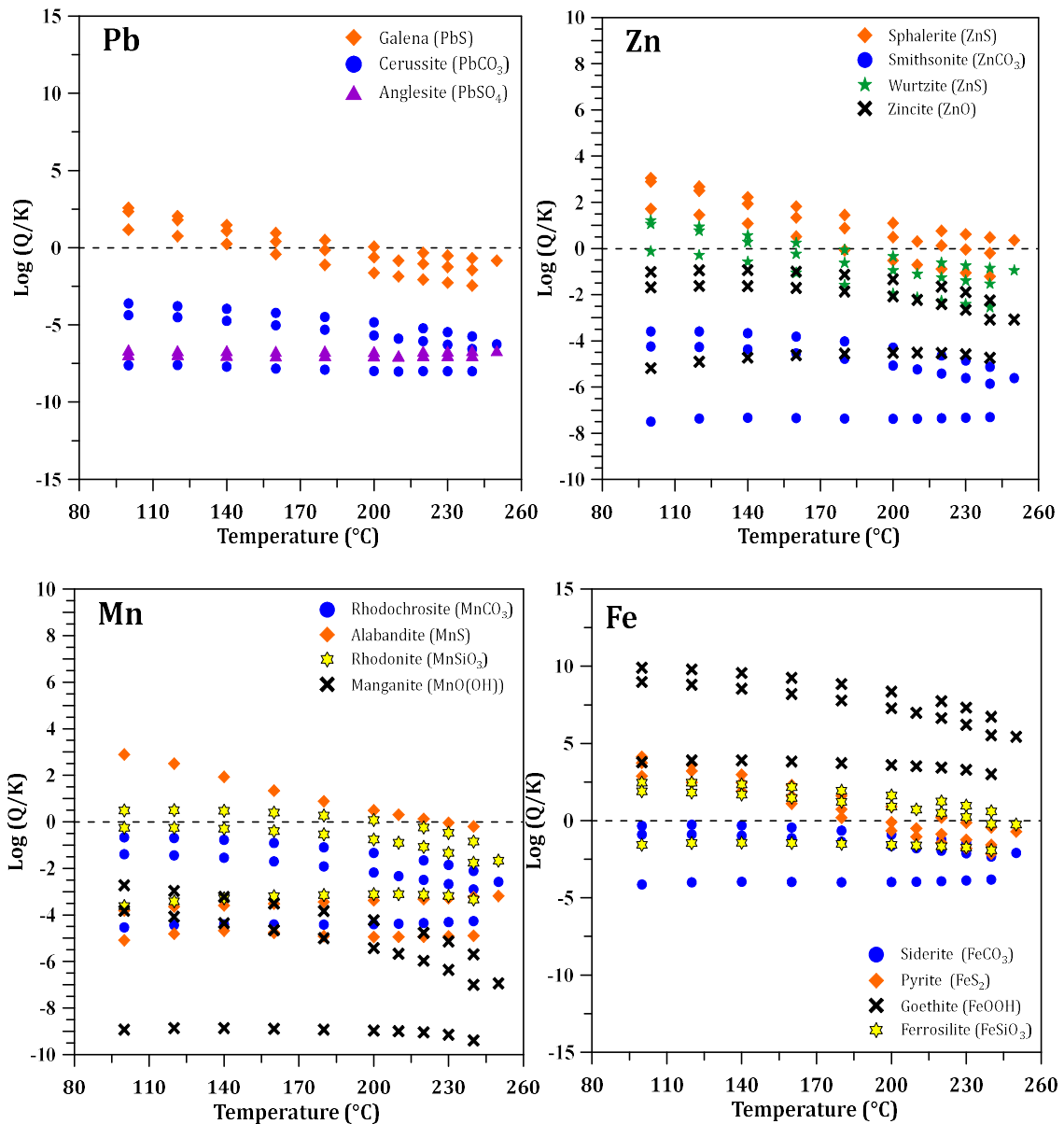


Figure 86: Mineral saturation of Assal 3 aquifer fluids with respect to Fe, Pb, Mn and Zn trace elements minerals. Different types of minerals are presented such as sulfide (in orange and green), oxide (in black), carbonate (blue circle) and silica (in yellow).

4.5 Comparison between similar fields

In this part of the study, the composition of deep fluids and scale minerals in the Assal geothermal field is compared to similar high-temperature saline geothermal fields such as Reykjanes (Iceland), Salton Sea (California), and Milos (Greece). The aim is to provide a general overview about the potential scaling in the Assal fluid.

Table 7: Comparison of downhole liquid composition in Reykjanes, Salton Sea, Milos, and Assal. Concentrations are given in ppm.

Sample N°	Iceland ⁽¹⁾	California ⁽²⁾	Greece ⁽³⁾	Djibouti
	Reykjanes RN-09	Salton Sea State 2-14	Milos Milos 2	Assal 3 A3-1
Depth (m)	1402	1850	1000	1316
T(°C)	295	223.4	310	251.3
pH	5	4.9	-	5.2
B	7.5	257	-	9.3
SiO ₂	594	461	491	471
Na	8,977	53,000	24,369	27,154
K	1292	16,700	6045	4567
Mg	0.8	33	18	22.1
Ca	1429	27,400	32,102	15,419
F	-	-	31	5
Cl	17,696	151,000	49,280	72,819
SO ₄	-	65	97	12.7
Al	0.1	-	0.02	1.5
Fe	0.4	1560	9	33.1
CO ₂	1067	1600	-	318.1
H ₂ S	27.1	15	-	0.5
NH ₃	-	-	-	5.8
TDS	232,204	256,000	-	119,349
H ₂	0.05	-	-	-
CH ₄	0.04	-	-	-
N ₂	6.6	-	-	-

(1) Modified from (Hardardóttir, 2011) ⁽¹⁾, calculated deep reservoir fluid using WATCH (Williams and McKibben, 1989) ⁽²⁾ and modified from (Christanis and Seymour, 1995) ⁽³⁾

Reykjanes, Iceland

The chemical composition of the geothermal fluid from well RN-09 is presented in Table 7. In this field, the scales observed from samples collected in 2000 to 2006 mainly consist of sulfides. At lower temperatures, the predominant scale is amorphous silica (Hardardóttir, 2011). Among the most common sulfides in Reykjanes, wurtzite is prevalent at higher pressures, while sphalerite is found at lower pressures, and traces of galena are detected at intermediate pressures. Additionally, traces of chalcopyrite and bornite have been observed in Reykjanes (Ármannsson, 2018).

The concentrations of Cu, Zn, Fe, and Pb in the pipelines exhibit variation depending on their location; low concentrations are found when pressure decreases. The concentrations of Ag and Au in the scales show a wide range, with their presence influenced by the location of precipitation. The highest concentrations of precious metals are found in surface pipelines at the orifice plate, where pressure experiences a sharp reduction (Hardardóttir, 2011).

A summary of the scales observed in this geothermal field is provided in Table 8.

Salton Sea, USA

The chemical composition of the geothermal fluid from well State 2-14 is presented in Table 7. The unusually high concentrations of Fe, Zn, and Mn in the geothermal brines of this field appear to play a significant role in controlling the rates of silica deposition. In addition, the highest deposition rate has been observed at pH 5-8, while the minimum rates occur at pH 1-3 (Hoffman, 1975). The iron-rich deposits contain high levels of Cu (20%) and Ag (6%) present as bornite (Cu_5FeS_4 or $(\text{Cu,Ag})_5\text{FeS}_4$), digenite (Cu_9S_5 or $(\text{Cu,Ag})_9\text{S}_5$), chalcopyrite (CuFeS_2), chalcocite (Cu_2S or $(\text{Cu,Ag})_2\text{S}$) and other sulfide minerals. (Skinner, et al., 1967).

A summary of the scales observed in this geothermal field is provided in Table 8.

Milos, Greece

The chemical composition of the geothermal fluid from well Milos 2 is presented in Table 7. The most abundant elements that have been identified from Milos are Si, Fe and Zn with lesser Pb, S, Ca and K, and the base metals occur as sulfides, bisulphites, or sulfates, and not as silicates. The scales consist of both amorphous/cryptocrystalline and crystalline phases that is mainly are base metal sulfides: sphalerite (ZnS), chalcopyrite (CuFeS_2) and galena (PbS) (Cullity, 1978) and that crystallinity increases towards the end of the reinjection line. Silica exists as an amorphous/cryptocrystalline phase (opal). Scale deposition was observed along the brine re-injection line, near the geothermal productive well, in the middle of the re-injection pipe and near the re-injection well (Christanis and Seymour, 1995).

Table 8: Comparison between the mineral depositions found in Reykjanes (Iceland); Salton Sea (California); Milos (Greece) and Assal (Djibouti).

Scale Mineral	Reykjanes ⁽¹⁾	Salton Sea ⁽²⁾	Milos ⁽³⁾	Assal
	Iceland	USA	Greece	Djibouti
Amorphous silica	✓	✓	✓	✓
Anglesite	✓			
Anhydrite	✓			
Bornite	✓	✓		
Calcite				✓
Chalcopyrite	✓	✓	✓	
Chalcocite				✓
Cotunnite	✓			
Covellite	✓			
Digenite	✓	✓		
Ferrosilite		✓	✓	✓
Galena	✓		✓	✓
Goethite	✓			
Gold	✓			
Halite	✓			
Hematite	✓		✓	
Magnetite	✓		✓	
Nantokite	✓			
Native silver	✓			
Pyrite	✓	✓	✓	
Pyrrhotite	✓	✓	✓	
Quartz				
Siderite			✓	
Sphalerite	✓		✓	✓
Sylvite	✓			
Troilite		✓		
Wurtzite	✓		✓	

(Hardardóttir, 2011) ⁽¹⁾, (Williams and McKibben, 1989) ⁽²⁾ and (Christanis and Seymour, 1995) ⁽³⁾

4.6 Mineral extraction

In addition to their role in electrical or heat generation, geothermal fluids can also serve as sources of various elements present in the brine. Geothermal fluids contain a numerous of chemical components, some of which have the potential to yield valuable metals and minerals. The relatively high concentration of Li, Pb, Mn, Zn and Fe, among others, in the Assal fluids could derive in economically viable mineral extraction.

Various processes for the treatment of geothermal fluids can be categorized into three main groups: absorption, concentration, and precipitation. These processes are often employed in a series (Climo et al. in 2015). Some specific methods used in this context include filtration, electrocoagulation, electrodialysis, and the use of ion exchange resins.

Extraction of lithium (Li), manganese (Mn) and zinc (Zn)

The extraction of Li as a coproduct of the produced geothermal brine can give further economic upswing to the utilization of geothermal energy. The increased demand for Li is driven by two types of battery uses: (1) the rapidly growing production of electric vehicles—many countries will require a switch to an all-electric vehicle fleet within the next 10–20 years, and (2) the increased demand for battery energy storage to offset the intermittent nature of important renewable energy sources, such as solar and wind (Stringfellow and Dobson, 2021).

Li co-occurs with many transition and post-transition metals in geothermal brines. Fe, Mn and Zn so called base metals which is present in high concentration can form scales or precipitates and can be toxic (e.g., Pb). Metal management, particularly when it comes to precipitates solids, can be expensive, especially if the metals contain toxic or regulated elements. Furthermore, the economics of Li recovery might be improved by the recovery of valuable metals in a purity or composition that is marketable. In 2021, the annual cost of battery-grade lithium carbonate in the Unites States was \$17,000 per ton (USGS, 2022).

The following factors should be considered when looking at Li recovery from brine from an economic standpoint:

1. The concentration of Li in brine
2. The ratio of alkali metals and alkaline earth elements to Li
3. The complexity of the phase chemistry

The most promising sources of Li in brines in the United States are the hypersaline geothermal brines from the Salton Sea. Research into the recovery of base metals from Salton Sea geothermal brines dates to the 1970s and 1980s, during which several projects were assessed at the laboratory scale, and a few progressed to pilot-scale testing. Li recovery from Salton Sea geothermal brines has also been investigated (Stringfellow and Dobson, 2021). Some methods for the recovery of Li are:

- Precipitation of Li with $AlCl_3$. The precipitation of Li with $AlCl_3$ has been proposed as a method for Li recovery. However, it is important to emphasize that for a

technique or method to be considered practical and valuable, it must be both environmentally sustainable and economically.

- Integrated Li Adsorption Desorption (ILiAD) is a technology that is currently in use as a marketing initiative to advance the extraction of Li from geothermal brines in Salton Sea. This process includes pretreatment, Li extraction, purification, and the production of Li products. The ILiAD process begins with the extraction and recovery of Fe, SiO₂, Zn, and Mn.
- Adsorption by metal oxides and hydroxides is the most technologically sophisticated and well-studied technique for directly extracting Li from brines.

Extraction of silica (SiO₂)

Geothermal fluid naturally contains silica, and due to changes in pressure and temperature, it can precipitate clogging of tanks, pipes, and other equipment. To address this issue, the geothermal industry has implemented a strategy to not only prevent clogs but also to generate a valuable by-product: silica. Furthermore, the extraction of silica from geothermal fluid enhances the extraction process of hot fluid from production wells. This not only reduces maintenance costs related to scaling in surface facilities and injection wells but also promotes the co-production of valuable minerals.

Some alternatives for the removal of silica are ageing or pond retention (Yanagase et al., 1970), crystallization/clarification (Featherstone, 1988), controlled precipitation by metals (Rothbaum and Anderton, 1975) and by chelating agents for Al-silicates (Gallup, 1997), among others.

Considering the composition in the fluids of the well Assal 3, the amount of mineral that can be obtained from the brine for a power plant of 50 MWe is presented in Table 9. The calculations were performed under the assumption of a 70% efficiency recovery, with each productive well anticipated to generate 6.25 MWe.

Table 9: Estimation of mineral/extraction from the Assal fluids.

	Conc in the fluid (ppm)	Total amount (t/month)
Li (as Li ₂ CO ₃)	15.6	68,900
SiO ₂	521.3	215,000
Mn (as MnO ₂)	131	86,000
Pb	1.4	581
Zn	41.9	17,300
Fe (as Fe ₂ O ₃)	36.6	43,000

Conclusions

The scaling potential of the high-temperature geothermal fluids from the Assal field were studied in order to determine potential challenges issues during utilization. Additionally, various methods for the extraction of valuable minerals have been proposed. Chemical data obtained from the well discharges, in particular well Assal 3, was used for this analysis. The reservoir fluid composition was determined by assuming an equilibration with quartz (245-251 °C). The calculated pH values ranged from 4.4 to 5.2 and the chlorine content was approximately 70,000 ppm. Based on this data, an evaluation of the reservoir fluid composition was conducted, and subsequently, both boiling and cooling models were proposed to obtain the saturation index of various minerals at different temperatures. The formation of these minerals at surface conditions were compared with the scales identified in the production tests conducted in the early 90s. Among the scales observed at surface, amorphous silica, galena and sphalerite shown supersaturation under surface conditions in the cooling model, while ferrosilite and calcite present a similar behaviour in the boiling model. Furthermore, the cooling model predicts the formation of minerals associated with the local lithology, such as illite, low albite, epidote, and pyrite. In contrast, the boiling model suggests the formation of minerals that are neither present in the observed scales nor part of the regional geology. Minerals containing Mn, Pb and Zn typically show undersaturation, except for the sulfide minerals, while Fe-bearing minerals may have a significant influence on the mineral deposition at surface. Apparently, the cooling model provides a better understanding of the mineral formation in these fluids.

In addition, the chemical composition of the Assal fluids and the scaling formation were compared to those of other high-temperature, high-salinity geothermal fluids such as those from Reykjanes, Salton Sea and Milos. Amorphous silica, chalcopyrite, pyrite, and pyrrhotite were identified as common scales in all those fields. While amorphous silica was also observed in Assal, pyrite was not identified in the scaling tests, but in the cooling model. Galena and sphalerite are the common sulfide scales except in Salton Sea which fluids present lower contents of Cl and SO₄. Pyrrhotite was neither identified in the scaling tests or the predicted in the models. The differences may result from different geological locations and species of the deep fluid.

Finally, it was estimated the potential extraction of Li (68,900 t/month), SiO₂ (215,000 t/month), Mn (86,000 t/month), Pb (581 t/month), Zn (17,300 t/month) and Fe (43,000 t/month) for commercial purposes in a 50 MW power plant. This aspect could play an important role in the economics and the feasibility assessment for future stages of the power plant construction and/or further development of the area.

References

- Alderson, C. (2023). *Geothermal: An environmentally friendly alternative to fossil fuel* (Thesis, Middle Tennessee State University). Available at: <https://jewlscholar.mtsu.edu/server/api/core/bitstreams/0588ba73-2f24-4cb2-9ac7-6f85533ae6bc/content>
- Árnórsson, S. (1969). A geochemical study of selected elements in thermal waters of Iceland. (PhD thesis, Imperial college, London), 353 p.
- Árnórsson, S. (1981). Mineral deposition from Icelandic geothermal waters, environmental and utilization problems. *J. Petroleum Technology*, 33-1, 181-187.
- Árnórsson, S., Sigurdsson, S. and Svavarsson, H., (1982). The chemistry of geothermal waters in Iceland I. Calculation of aqueous speciation from 0°C to 370°C. *Geochim. Cosmochim. Acta*, 46, 1513-1532.
- Árnórsson, S. (1989). Deposition of calcium carbonate minerals from geothermal waters-theoretical considerations. *Geothermics*, 18, 33-39.
- ASTM (1966). Manual on industrial water and industrial waster water. 2nd Edition. *Am. Soc. for testing materials*, Philadelphia.
- Aquater (1989). *Djibouti geothermal exploration project. Republic of Djibouti, final report.* Aquater, report, 159 pp.
- APHA (1985). *Standard methods for the examination of water and waste (16th ed.)*. Washington, 1268 pp.
- Ármannsson, H. (1981). Analysis of mercury in geothermal fluids. *Proc. 8th Nordic Trace element and microchemistry conference, Sandefjord, Norway*, 10.
- Ármannsson, H. (2018). An overview of carbon dioxide emissions from Icelandic geothermal areas. *Applied Geochemistry*, 97, 11-18.
- Ármannsson, H., and Hardardóttir, V. (2010). Geochemicqal patterns in saline high temperature geothermal systems. In Birkle, P., and Torres-Alvarando, I.S. (Eds.), *Water-rock interaction*. CRC Press, Taylor and Francis Group, London, 133-136. Available at: <https://bit.ly/3PL6OSO>
- Ármannsson, H., Sigurðsson, Ó., Matthíasson, M., and Árnason, K. (1990). *Well Tests in Asal, Djibouti and Possible Continued Exploration (lecture)*. Iceland GeoSurvey, Grensásvegur 9, IS-108, Reykjavík, Iceland. Available at: <https://bit.ly/3JLFj7w>
- Ármannsson, H. and Hauksson, T. (1978). *On sodium determination (in Icelandic)*. Orkustofnun, Report No. OS JHD 7815, 8 pp.
- Barberi, F., Borsi, S., Ferrara, G., Marinelli G., and Varet J. (1970). Relations between Tectonics and Magmatology in the Northern Danakil Depression (Ethiopia). *Phi. Trans. Roy. Soc. Lond. A, Mathematical and Physical Sciences*, 267, a Discussion on

the Structure and Evolution of the Red Sea and the Nature of the Red Sea, Gulf of Aden and Ethiopia Rift Junction, 293-311 pp.

- Battisteili, A., Rivera, R.J., Celati, R. and Mohamed, A. (1990). Study of the Effect of Several Wellbore Conditions on the Output Characteristics of Wells at the Asal Field, Republic of Djibouti. *Proceedings, Fifteenth Workshop on Geothermal Reservoir Engineering, Stanford University, Stanford, California*. SGP-TR130, 71-79.
- Battistelli, A., Rivera, J., and Ferragina, C. (1991). Reservoir engineering studies at the Asal field: Republic of Djibouti. *Geothermal Resources Council Bulletin*, 20(10), 280-289.
- Bjarnason, J.Ö. (2010). *The chemical speciation program WATCH, version 2.4*. ÍSOR – Iceland GeoSurvey, Reykjavik, website: www.geothermal.is/software
- Bosch B., Deschamps J., Lopoukhine M., Marce A. et Vilbert C. (1974). La zone géothermique du lac Asal (TFAI). Résultats de terrain et études expérimentales. *Bull. BRGM. II4*. 367-383.
- Bourcier, W.L., Lin, M., and Nix, G. 2005. Recovery of Minerals and Metals from Geothermal Fluids. *SME Annual meeting, Cincinnati, OH, United States*. 19 p.
- Brown, K., and Dunstall, M., (2000). Silica scaling under controlled hydrodynamic conditions. *Proceedings of the World Geothermal Congress 2000, Japan*. 6 p.
- Carver, C.T., Garg, S.K., Davis, L.C., and Jalludin, M. (2019). Reservoir Characterization from Exploration Well Completion Tests in the Fiale Caldera, Djibouti. *GRC Transactions, Vol. 43*, 14 p.
- Cheik, H.S. (2010). *Prefeasibility Design of a 2×25 MW Single-Flash Geothermal Power Plant in Asal, Djibouti*. United Nations University Geothermal Training Programme, Orkustofnun, Grensasvegur 9, IS-108 Reykjavik, Iceland, 22 p
- Christanis, K., and Seymour, K.St., (1995). A study of scale deposition: An analogue of meso- to epithermal ore formation in the volcano of Milos, Aegean arc, Greece. *Geothermics* 24, 541–552. [https://doi.org/10.1016/0375-6505\(95\)00006-C](https://doi.org/10.1016/0375-6505(95)00006-C)
- Corsi, R. (1986). Scaling and corrosion in geothermal equipment: problems and preventive measures. *Geothermics*, 15, (5–6), 1986, 839-856.
- Cullity, B.D., (1978). *Chemical analysis by X-ray diffraction*. Elements of X-Ray Diffraction, 2nd edition, 397-420.
- D'Amore, F., Giusti, D., and Abdallah, A. (1998). Geochemistry of the high-salinity geothermal field of Asal, Republic of Djibouti, Africa. *Geothermics*, 27(2), 197–210. Available at: [https://doi.org/10.1016/S0375-6505\(97\)10009-8](https://doi.org/10.1016/S0375-6505(97)10009-8)
- Dove, P.M., and Rimstidt J.D. (1994). Silica-Water Interactions. *Reviews in Mineralogy and Geochemistry* 29, no. 8 (n.d.): 259–308.
- Ellis, A.J. and Mahon, W.A.J. (1977). *Chemistry and geothermal systems*. academic Press. New York, 392 pp.

- Elisson, G. (1969). *Studies on silica in hot spring water from some high temperature areas (in Icelandic)*. A report. University of Iceland, Science Institute, 31 pp.
- Featherstone, J.L. (1988). *Process for removing silica from silica-rich geothermal brine*. US Patent 4,765,913.
- Fouillac, C., Fabriol, R., and Lundt, F., (1983). *Champ Géothermique d'Asal. Synthèse des données disponibles au 1er Janvier*. Rapport BRGM83-SGN-022-GTH, 71 p.
- Fontes, J., Siché M., Pouchan, P., and Zuppi, G.M. (1989). Teneurs en brome et chlore du lac Asal (Djibouti) et bilan en eau et en sels d'un système évaporitique complexe. *C.R. Acad. Sci. Paris 309 II*, 701-706.
- Fournier, R.O., and Rowe, J.J., (1966). Estimation of underground temperatures from the silica contents of water from hot springs and wet steam wells. *Am. J. Sci.*, 264, 685-697.
- Global volcanism program, (1978). *Report on Ardoukoba (Djibouti)*. (Squires, D., ed.). Scientific Event Alert Network Bulletin, 3:12. Smithsonian Institution, Global volcanism program.
- Grinstead, R., and Snider, S. (1967). Modification of the curcumin method for low level boron determination. *Analyst*, 92, 532-533.
- Gallup, D., (1997). Aluminium silicate scale formation and inhibition: Scale characterization and laboratory experiments. *Geothermics*, 26, No. 4, 483-499 pp
- Gallup, D., (1998). Geochemistry of Geothermal Fluids and Well Scales, and Potential for Mineral Recovery. *Ore Geology Reviews*, 12, 225-236.
- Graham, G.M., Boak, L.S., Sorbie, K.S., (2003). The influence of formation calcium and magnesium on the effectiveness of generically different barium sulfate oilfield scale inhibitors. *SPE Prod. Facil.* 18, 28-44.
- Gunnarsson, I., and Arnórsson, S., (2005). Impact of silica scaling on the efficiency of heat extraction from high-temperature geothermal fluids. *Geothermics*, 34, 320-329.
- Gunnlaugsson, E. (2012). Scaling in Geothermal Installation in Iceland. *Presented at "Short Course on Geothermal Development and Geothermal Wells"*, organized by UNU-GTP and LaGeo, in Santa Tecla, El Salvador, 6 p.
- Gunnlaugsson, E., Ármannsson, H., Thorhallson, S., Steingrímsson, B. (2014) Problems in Geothermal Operation-Scaling and Corrosion. *Presented at "Short Course VI on Utilization of Low- and Medium-Enthalpy Geothermal Resources and Financial Aspects of Utilization"*, organized by UNU-GTP and LaGeo, in Santa Tecla, El Salvador, March 23-29, 2014.
- Haga, A.O. (2015). Active Geothermal Systems and Related Epithermal Mineralizations in the Djibouti Republic. *Proceedings of the World Geothermal Congress 2015, Melbourne, Australia*, 10 p.

- Hardardóttir, V. (2011). *Metal-rich Scales in the Reykjanes Geothermal System, SW Iceland: Sulfide Minerals in a Seawater-dominated Hydrothermal Environment* (PhD thesis, Université d'Ottawa / University of Ottawa). 4543. Available at: <https://doi.org/10.20381/ruor>
- Hardardóttir, V., Ármannsson, H., and Thórhallsson, S. (2005). Characterization of Sulfide-Rich Scales in Brine at Reykjanes. *Proceedings of the World Geothermal Congress 2005, Antalya, Turkey, CD*, 8 pp.
- Hassan, A.A., Raymond, J., Giroux, B., and Sanjuan, B. (2021). New Insights into Hydrothermal Fluid Circulation Affected by Regional Groundwater Flow in the Asal Rift, Republic of Djibouti. *Energies*, 14(4), 1166 p. Available at: <https://doi.org/10.3390/en14041166>
- Hauksson, T. (1981). *Instructions for the use of Carle AGC III H, S gas chromatograph (in Icelandic)*. Orkustofnun, Report No. TH-81/03, 18 pp.
- Hjartarson, G., Gísladóttir, V., Gíslason, G., and Ólafsson, K. (2010). Geothermal Development in the Assal Area Djibouti. *Proceedings of the World Geothermal Congress 2010 Bali, Indonesia*, 8 p.
- Houmed, A.M., Haga, A.O., Abdilahi, S., and Varet, J. (2012). The Asal Geothermal Site, Djibouti Republic (Model Update, 2012). *Proceedings of the 4th African Rift Geothermal Conference Nairobi, Kenya*, 9 p.
- Houssein, D.E. and Axelsson, G. (2010). Geothermal resources in the Asal Region, Republic of Djibouti: An update with emphasis on reservoir engineering studies. *Geothermics*, 39(3), 220–227. Available at: <https://doi.org/10.1016/j.geothermics.2010.06.006>
- Koroleff, F. (1981 a). Determination of ammonia. In Grasshoff, K., Erhardt, M. and Kremling, K. (Eds.), *Methods of seawater analysis*, 150-157. Verlag chemie, Weinheim.
- Koroleff, F. (1983 b). Iron (by spectrophotometry). In Grasshoff, K., Erhardt, M. and Kremling, K. (Eds.), *Methods of seawater analysis*, 236-239. Verlag chemie, Weinheim.
- Koroleff, F. (1983 c). Manganese (by spectrophotometry). In Grasshoff, K., Erhardt, M. and Kremling, K. (Eds.), *Methods of seawater analysis*, 239-242. Verlag chemie, Weinheim.
- Hydes and Liss (1976). In Virkir-Orkint 1990: *Djibouti. Geothermal scaling and corrosion study. Final report*. Virkir-Orkint, Reykjavík, report, 273 pp.
- Le Gall, B., Daoud, A.M., Maury, R., Gasse, F., Rolet, J., Jalludin, M., Caminiti, A.-M., Moussa N. (2015). *Geological map of the republic of Djibouti*. Centre d'Etude et de Recherche de Djibouti (CERD) and CCGM 2015.
- Lopoukhine, M. (1973). *Etude thermométrique de la région du lac Asal*. Campagne 1972-1973. BRGM/73-SGN-139-GTH, 32 p.

- Mahon, W.A.J. (1966). Silica in hot water discharged from drillholes at Wairakei, New Zealand. *N. Z. J. Sci.*, 9, 135-144.
- Moore, G.L. (1989). *Introduction to inductively coupled plasma atomic emission spectrometry*. Elsevier, Amsterdam, 349.
- Mroczek, E., Carey, B., Climo, M., Li, Y. (2015). Technology review of mineral extraction from separated geothermal water, GNS Science Report 2015/25. 32 p.
- Ólafsson, J. (1974). Determination of nanogram quantities of mercury in seawater. *Anal. Chim. Acta*, 68, 207-211.
- Parkhurst, D.L. and Appelo, C.A.J. (1999). *User's guide to PHREEQC (version 2) - A computer program for speciation, batch-reaction, one-dimensional transport, and inverse geochemical calculations*. U.S. Department of the Interior, U.S. Geological Survey. Water-Resources Investigations Report 99-4259. Denver, Colorado. 326 p.
- Richter, A. (2021, 11 February). *KenGen bags drilling contract for geothermal project in Djibouti*. ThinkGeoEnergy. <https://www.thinkgeoenergy.com/kengen-wins-geothermal-drilling-contract-for-three-wells-in-djibouti/> (accessed 4.10.21).
- Rothbaum, H.P., and Anderton, B.H., (1975). Removal of silica and arsenic from geothermal discharge waters by precipitation of useful calcium silicates. *Proceedings: Second United Nations Symposium on the Development and Use of Geothermal Resources. San Francisco, California, 1975*. 1417-1425 pp.
- Sanjuan, B. (2010). Use of a new Sodium/Lithium (Na/Li) geothermometric relationship for High-Temperature (HT) geothermal fluids derived from seawater/basalt interaction processes: Application to the Djibouti case. *Proceedings of the Third East African Rift Geothermal Conference ARGEO-C3. Exploring and harnessing the renewable and promising geothermal energy*, 23 p.
- Sanjuan, B., Michard, G. and Michard, A. (1990). Origin of dissolved substances in the waters of thermal springs and boreholes of the Asal-Ghoubbet region (Republic of Djibouti) (In French. Origine des substances dissoutes dans les eaux des sources thermales et des forages de la région Asal-Ghoubbet (République de Djibouti)). *Journal of Volcanology and Geothermal Research*, 43(1-4), 333-352. Available at: [https://doi.org/10.1016/0377-0273\(90\)90060-S](https://doi.org/10.1016/0377-0273(90)90060-S)
- Skinner, B. J., White, D. E., Rose H. J. and Mays R. E. (1967). Sulfides Associated with the Salton Sea Geothermal Brine. *Econ. Geol.* 62, 316.
- Sigfússon, B., and Gunnarsson, I. (2011). Scaling prevention experiments in the Hellisheidi power plant, Iceland. *Proceedings of the 36th Workshop on Geothermal Reservoir Engineering, Stanford University, Stanford, California*, 5 pp.
- Stefán, A. and Sven, S. (1982). The chemistry of geothermal waters in Iceland. I. Calculation of aqueous speciation from 0° to 370°C. *Geochimica et Cosmochimica Acta* Vol. 46 pp. 1513 to 1532.

- Stringfellow, W.T., and Dobson, P.F. (2021). Technology for the Recovery of Lithium from Geothermal Brines. *Energies* 2021, 14, 6805. <https://doi.org/10.3390/en14206805>
- Tassew, M. (2001). *Effect of solid deposition on geothermal utilization and methods of control. Report 13 in: Geothermal training in Iceland 2001*. UNU-GTP, Iceland, 291-310.
- Tazieff, H., Varet, J., Barberi, F., and Giglia, G. (1972). Tectonic Significance of the Afar (or Danakil) Depression. Tectonic Significance of the Afar (or Danakil) Depression. *Nature* 235, 144–147. <https://doi.org/10.1038/235144a0>
- Thorbjörnsson, D., Hersir, G.P., Gałeczka, I.M., and Richter, B. (2017). *Assal geothermal area, Djibouti, Conceptual Model*. ÍSOR - Iceland GeoSurvey, report ÍSOR-2017/089, 17-0091, 76 pp.
- Toba, A.L., Nguyen, R.T., Cole, C., Neupane, G., Paranthaman, M.P., 2021. U.S. lithium resources from geothermal and extraction feasibility. *Resour. Conserv. Recycl.* 169, 105514.
- Turk, J., Haizlip, Jill., Mohamed, J., Mann, Mary., Letvin, A., and Moussa, N. (2019). A Comparison of Alteration Mineralogy and Measured Temperatures from Three Exploration Wells in The Fiale Caldera, Djibouti. *GRC Transactions*, 43, 11 p.
- USGS, (2022). Mineral Commodity Summaries. *U.S. Geological Survey, Mineral Commodity Summaries, January 2022, Lithium*. <https://pubs.usgs.gov/periodicals/mcs2022/mcs2022-lithium.pdf>
- Van den Heuvel, D., Gunnlaugsson, E., Gunnarsson, I., Stawski, T., Peacock, C., Benning, L., (2018). Understanding amorphous silica scaling under well-constrained conditions inside geothermal pipelines. *Geothermics* 76, 231-241
- Varet, J. (1978). *The geology of central and southern Afar (Ethiopia and Djibouti republic)*. 1/500.000 map and report. CNRS, Paris 124 p.
- Varet, J. (2014). Asal-Fialé geothermal field (Djibouti republic): A new interpretation for a geothermal reservoir in an actively spreading rift segment. *Proceedings 5th African Rift geothermal Conference Arusha, Tanzania*, 29-3, 9 p.
- Virkir-Orkint (1990). *Djibouti. Geothermal scaling and corrosion study. Final report*. Virkir-Orkint, Reykjavík, report, 273 pp.
- Warren, I. (2021). Techno-Economic Analysis of Lithium Extraction from Geothermal Brines. Golden, CO: National Renewable Energy Laboratory. NREL/TP-5700-79178.
- Willis, W.J. (1961). Determination of calcium and magnesium in urine by atomic absorption spectroscopy. *Anal. Chem.*, 33, 556 p.
- Williams, A.E., and McKibben, M.A., (1989). A brine interface in the Salton Sea Geothermal System, California: Fluid geochemical and isotopic characteristics. *Geochimica et Cosmochimica Acta* 53, 1905–1920. [https://doi.org/10.1016/0016-7037\(89\)90312-8](https://doi.org/10.1016/0016-7037(89)90312-8)

- Thorbjörnsson, D., Hersir, G.P., Richter, B., and Galeczka, I.M. (2017). *Lake Assal- A preliminary conceptual model (No. 17-0091)*. Internal report. Iceland GeoSurvey.
- Yanagase, T., Suginoara, Y., and Yanagase, K. (1970). The Properties of Scales and Methods to prevent them. *Geothermics 2*, 1619 – 1623.
- Zhao, H., Huang, Y., Deng, S., Wang, L., Peng, H., Shen, X., Ling, D., Liu, L., Liu, Y. (2022). Research progress on scaling mechanism and anti-scaling technology of geothermal well system. *Journal of Dispersion Science and Technology*, 44:9, 1657-1670. <https://doi.org/10.1080/01932691.2022.2033625>
- Zotzmann, J., Vetter, A., Regenspurg, S. (2018). Evaluating efficiency and stability of calcite scaling inhibitors at high pressures and high temperatures in laboratory scale. *Geoth. Energy 6*, 18.
- Zotzmann, J., Feldbusch, E., Kruppke, I., Aibibu, D., Regenspurg, S. (2023). Removal of lead and copper ions from geothermal brine at various temperatures and salinities using chemically crosslinked chitosan. *Applied Geochemistry 155* (2023) 105733. <https://doi.org/10.1016/j.apgeochem.2023.105733>

Appendix A – Chemical composition of the scaling encountered in the well Assal 3 (Haga, 2015)

Scaling at the wellhead of Assal 3

Constituent	WELLHEAD
P (bar)	20
SiO ₂ (%)	19.6
Al ₂ O ₃ (%)	3.7
Fe ₂ O ₃ (%)	22.5
Mno (%)	2.3
Mgo (%)	1.6
Cao (%)	0.6
Na ₂ O (%)	4.4
K ₂ O (%)	0.1
S (%)	13.7
CU (%)	0.4
Pb (%)	22.3
Zn (%)	8.8

Appendix B – Temperature equations for equilibrium constants for individual mineral dissolution reactions. The log K is valid in the range 0-300°C (Parkhurst and Appelo, 1999)

Mineral	Abbreviation	Dissolution reaction	Log K (Tin K)	
1	Am -SiO ₂	sil	SiO ₂ + 2H ₂ O = H ₄ SiO ₄	+1.2109 + 7.0767*10 ⁻³ *T + 2363.4/T - 3.4449*logT -485910/T ²
2	Anhydrite*	anh	CaSO ₄ = Ca ⁺² + SO ⁻² ₄	-209.86 -7.8823 *10 ⁻² *T + 5096.9 /T + 85.642 *logT – 79.594 /T ²
3	Alunite	alu	KAl ₃ (OH) ₆ (SO ₄) ₂ + 6H ⁺ ↔ K ⁺ + 2SO ₄ ⁻² + 3Al ⁺³ + 6H ₂ O	-685.81 - 0.22455*T + 2.6886*10 ⁴ /T + 267.58*logT + 419.73/T ²
4	Aragonite	ara	CaCO ₃ = Ca ⁺² + CO ⁻³	- 149.34 - 4.8043*10 ⁻² *T + 4908.9/T + 60.284*logT + 76.644/T ²
5	Barite	bar	BaSO ₄ = Ba ⁺² + SO ⁻² ₄	-187.47 - 7.5521*10 ⁻² *T + 2079/T + 77.998*logT + 32.497/T ²
6	Calcite	cal	CaCO ₃ + 2H ⁺ = Ca ⁺² + H ₂ O(l) + CO ₂ (aq)	-149.78 - 4.8370*10 ⁻² *T + 4897.4/T + 60.458*logT + 76.464/T ²
7	Chalcedony	chal	SiO ₂ + 2H ₂ O = H ₄ SiO ₄	-9.0068 + 9.3241*10 ⁻³ *T + 4053.5/T + 55.963*logT - 7.5077*10 ⁵ /T ²
8	Cristobalite alpha	cris-α	SiO ₂ = SiO ₂	-11.936 + 9.0520*10 ⁻³ *T + 4370.1/T - 0.11464*logT - 7.6568*10 ⁵ /T ²
9	Cristobalite beta	cris-β	SiO ₂ = SiO ₂	-4.7414 + 9.7567*10 ⁻³ *T + 3883.1/T - 2.583*logT - 9.9636*10 ⁵ /T ²
10	Dolomite	dol	CaMg(CO ₃) ₂ = Ca ⁺² + Mg ⁺² + 2CO ⁻² ₃	- 317.82 - 9.8179*10 ⁻² *T + 10845/T + 126.57*logT + 169.32/T ²
11	Epidote	epi	Al ₂ FeSi ₃ O ₁₂ (OH) + 12H ₂ O(l) = 2Ca ⁺² + Fe(OH) ₄ ⁻ + 2Al(OH) ₄ ⁻ + 3H ₄ SiO ₄ 0 + OH ⁻	- 26.187- 3.6436*10 ⁻² *T + 19351/T + 3.3671*logT - 303190/T ²
12	Ferrosilite	fer	FeSiO ₃ = FeO + SiO ₂	+9.0041 + 3.7917*10 ⁻³ *T + 5162.5/T - 6.3009*logT - 395650/T ²
13	Galena	gal	PbS + H ⁺ = Pb ⁺² + HS ⁻	-121.24 - 4.3477*10 ⁻² *T - 1646.3/T + 50.454*logT - 0.2654/T ²
14	Gypsum	gyp	Ca ⁺² + SO ⁻² ₄ + 2H ₂ O	-24.416 + 1.4646 *10 ⁻² *T + 16181 /T + 2.3723 *logT - 1536900 /T ²
15	Goethite	goe	FeO(OH) + 3H ⁺ = Fe ⁺³ + 2H ₂ O	-60.331 - 1.0847*10 ⁻² *T + 4775.9/T + 19.429*logT + 81.122/T ²

(cont..)

Mineral	Abbreviation	Dissolution reaction	Log K (Tin K)	
16	Hematite	hem	$\text{Fe}_2\text{O}_3 + 6\text{H}^+ = 2\text{Fe}^{+3} + 3\text{H}_2\text{O}$	$-220.15 - 6.0290 \cdot 10^{-2} \cdot T + 11812/T + 80.253 \cdot \log T + 184.38/T^2$
17	Illite	ill	$\text{K}_6\text{Mg}_{25}\text{Al}_6\text{Si}_{15}\text{O}_{10}(\text{OH})_2 + 8\text{H}^+ + 2\text{H}_2\text{O} = 6\text{H}^+ + 25\text{Mg}^{+2} + 6\text{Al}^{+3} + 15\text{H}_4\text{SiO}_4$	$+26.069 - 1.2553 \cdot 10^{-3} \cdot T + 13670/T - 20.232 \cdot \log T - 1120400/T^2$
18	Low albite	alb	$\text{alb (low)} + 8\text{H}_2\text{O} = \text{Na}^+ + \text{Al}(\text{OH})_4^- + 3\text{H}_4\text{SiO}_4$	$-12.860 + 1.4481 \cdot 10^{-2} \cdot T + 13913/T - 6.9417 \cdot \log T - 1625600/T^2$
19	Magnetite	mag	$\text{Fe}_3\text{O}_4 + 4\text{H}_2\text{O(l)} = \text{Fe}^{+2} + 2\text{Fe}(\text{OH})_4^-$	$-305.1 - 7.9919 \cdot 10^{-2} \cdot T + 18709/T + 111.78 \cdot \log T - 292.03/T^2$
20	Pyrite	pyr	$\text{FeS}_2 + 2\text{H}^+ + \text{H}_2(\text{aq}) = \text{Fe}^{+2} + 2\text{H}_2\text{S}^0_{(l)}$	$-241.95 - 8.7948 \cdot 10^{-2} \cdot T - 629.11/T + 99.248 \cdot \log T - 9.7454/T^2$
21	Pyrrhotite	pyrr	$\text{FeS} + 2\text{H}^+ = \text{Fe}^{+2} + \text{H}_2\text{S}(\text{aq})$	$-157.85 - 5.2258 \cdot 10^{-2} \cdot T + 3971.1/T + 63.195 \cdot \log T + 62.012/T^2$
22	Quartz	qtz	$\text{SiO}_2 + 2\text{H}_2\text{O} = \text{H}_4\text{SiO}_4$	$+7.7698 \cdot 10^{-2} + 1.0612 \cdot 10^{-2} \cdot T + 3465.1/T - 4.3551 \cdot \log T - 721380/T^2$
23	Siderite	sid	$\text{FeCO}_3 = \text{Fe}^{+2} + \text{CO}_3^{-2}$	$-159.90 - 4.9361 \cdot 10^{-2} \cdot T + 5494.7/T - 63.032 \cdot \log T + 85.787/T^2$
24	Sphalerite	sph	$\text{ZnS} + \text{H}^+ = \text{HS}^- + \text{Zn}^{+2}$	$-154.97 - 4.8953 \cdot 10^{-2} \cdot T + 1785.0/T + 61.472 \cdot \log T + 27.899/T^2$
25	Troilite	tro	$\text{FeS} + \text{H}^+ = \text{Fe}^{+2} + \text{HS}^-$	$-161.46 - 5.3170 \cdot 10^{-3} \cdot T + 4046.1/T + 64.62 \cdot \log T + 63.183/T^2$
26	Witherite	wit	$\text{BaCO}_3 = \text{Ba}^{+2} + \text{CO}_3^{-2}$	$-159.90 - 4.9361 \cdot 10^{-2} \cdot T + 5494.7/T - 63.032 \cdot \log T + 85.787/T^2$